ADVANCING EARTH AND SPACE SCIENCES

JGR Biogeosciences

RESEARCH ARTICLE

10.1029/2025JG008806

Optimizing the Temperature Sensitivity of the Isoprene Emission Model MEGAN in Different Ecosystems Using a Metropolis-Hastings Markov Chain Monte Carlo Method

C. A. DiMaria[1], D. B. A. Jones[1], V. Ferracci[2,3], A. A. Bloom[4], H. M. Worden[5], R. Seco[6], L. Vettikkat[7], A. M. Yáñez-Serrano[6,8,9], A. B. Guenther[10], A. Araujo[11], A. H. Goldstein[12,13], B. Langford[14], J. Cash[14], N. R. P. Harris[2], L. Brown[15], R. Rinnan[16], S. Schobesberger[7], T. Holst[17], and J. E. Mak[18]

[1]Department of Physics, University of Toronto, Toronto, ON, Canada, [2]Cranfield Environment Centre, Cranfield University, Cranfield, UK, [3]National Physical Laboratory, Teddington, UK, [4]Jet Propulsion Laboratory, California Institute of Technology, Pasadena, CA, USA, [5]Atmospheric Chemistry Observations & Modeling Laboratory, National Center for Atmospheric Research, Boulder, CO, USA, [6]Institute of Environmental Assessment and Water Research (IDAEA-CSIC), Barcelona, Spain, [7]Department of Technical Physics, University of Eastern Finland, Kuopio, Finland, [8]CREAF, Barcelona, Spain, [9]CSIC, Global Ecology Unit, CREAF-CSIC-UAB, Barcelona, Spain, [10]Department of Earth System Science, University of California, Irvine, CA, USA, [11]Empresa Brasileira de Pesquisa Agropecuária (Embrapa) Amazonia Oriental, Belém, Brazil, [12]Department of Environmental Science, Policy, and Management, University of California Berkeley, Berkeley, CA, USA, [13]Department of Civil and Environmental Engineering, University of California Berkeley, Berkeley, CA, USA, [14]UK Centre for Ecology & Hydrology, Bush Estate, Penicuik, UK, [15]School of Science, Engineering & Environment, University of Salford, Manchester, UK, [16]Department of Biology, University of Copenhagen, Copenhagen, Denmark, [17]Department of Physical Geography and Ecosystem Science, Lund University, Lund, Sweden, [18]School of Marine and Atmospheric Sciences, Stony Brook University, Stony Brook, NY, USA

Key Points:

- Measurements show that the sensitivity of biogenic isoprene emission rates to temperature varies widely across different ecosystems
- Emission rates at some high-latitude sites were up to 4 times more sensitive to temperature than predicted by the widely used MEGAN model
- Optimizing the empirical parameters in MEGAN with observations yields improved isoprene emission estimates during high-temperature periods

Supporting Information:

Supporting Information may be found in the online version of this article.

Correspondence to:

C. A. DiMaria,
christian.dimaria@mail.utoronto.ca

Citation:

DiMaria, C. A., Jones, D. B. A., Ferracci, V., Bloom, A. A., Worden, H. M., Seco, R., et al. (2025). Optimizing the temperature sensitivity of the isoprene emission model MEGAN in different ecosystems using a Metropolis-Hastings Markov Chain Monte Carlo method. *Journal of Geophysical Research: Biogeosciences*, *130*, e2025JG008806. https://doi.org/10.1029/2025JG008806

Received 30 JAN 2025
Accepted 24 APR 2025

Author Contributions:

Conceptualization: C. A. DiMaria, D. B. A. Jones, V. Ferracci, A. A. Bloom, H. M. Worden, R. Seco, L. Vettikkat, A. M. Yáñez-Serrano, A. B. Guenther
Data curation: V. Ferracci, H. M. Worden, R. Seco, L. Vettikkat, A. M. Yáñez-Serrano, A. B. Guenther, A. Araujo, A. H. Goldstein, B. Langford, J. Cash, N. R. P. Harris, L. Brown, R. Rinnan, S. Schobesberger, T. Holst, J. E. Mak
Formal analysis: C. A. DiMaria
Investigation: C. A. DiMaria, V. Ferracci, H. M. Worden, R. Seco, L. Vettikkat,

Abstract

Isoprene is a reactive hydrocarbon emitted to the atmosphere in large quantities by terrestrial vegetation. Annual total isoprene emissions exceed 300 Tg a^{-1}, but emission rates vary widely among plant species and are sensitive to meteorological and environmental conditions including temperature, sunlight, and soil moisture. Due to its high reactivity, isoprene has a large impact on air quality and climate pollutants such as ozone and aerosols. It is also an important sink for the hydroxyl radical which impacts the lifetime of the important greenhouse gas methane along with many other trace gas species. Modeling the impacts of isoprene emissions on atmospheric chemistry and climate requires accurate isoprene emission estimates. These can be obtained using the empirical Model of Emissions of Gases and Aerosols from Nature (MEGAN), but the parameterization of this model is uncertain due in part to limited field observations. In this study, we use ground-based measurements of isoprene concentrations and fluxes from 11 field sites to assess the variability of the isoprene emission temperature response across ecosystems. We then use these observations in a Metropolis-Hastings Markov Chain Monte Carlo (MHMCMC) data assimilation framework to optimize the MEGAN temperature response function. We find that the performance of MEGAN can be significantly improved at several high-latitude field sites by increasing the modeled sensitivity of isoprene emissions to past temperatures. At some sites, the optimized model was nearly four times more sensitive to temperature than the unoptimized model. This has implications for air quality modeling in a warming climate.

Plain Language Summary

Many species of plants emit a reactive gas called isoprene in response to environmental stressors. Isoprene is emitted in large quantities globally and readily reacts with other gases in the atmosphere to produce pollutants like ground-level ozone and aerosols, which impact both air quality and climate. Emission rates are highly variable among plant species and are very sensitive to temperature, with rates increasing exponentially during hot weather. Current models of isoprene emissions appear to underestimate the temperature sensitivity of emissions for some plant species, espcially in high-latitude regions like the Arctic. In this study, we used measurements from a diverse range of ecosystems around to the world to quantify the temperature sensitivity of isoprene emissions and compare with the predictions of a widely used isoprene emission model. We found that model performed well in many ecosystems but underestimated the temperature sensitivity in several locations, including temperate forests and high-latitude tundra where the measured temperature sensitivity was up to four times greater than model predictions. We used the observations to optimize parameters in the model, and found that this greatly improved model

A. M. Yáñez-Serrano, A. B. Guenther, A. Araujo, A. H. Goldstein, B. Langford, J. Cash, N. R. P. Harris, L. Brown, R. Rinnan, S. Schobesberger, T. Holst, J. E. Mak
Methodology: C. A. DiMaria, D. B. A. Jones, V. Ferracci, A. A. Bloom, H. M. Worden, R. Seco, A. M. Yáñez-Serrano, A. B. Guenther
Resources: D. B. A. Jones
Software: C. A. DiMaria, A. A. Bloom
Supervision: D. B. A. Jones, H. M. Worden
Visualization: C. A. DiMaria
Writing – original draft: C. A. DiMaria, D. B. A. Jones
Writing – review & editing: C. A. DiMaria, D. B. A. Jones, V. Ferracci, A. A. Bloom, H. M. Worden, R. Seco, L. Vettikkat, A. M. Yáñez-Serrano, A. B. Guenther, A. Araujo, A. H. Goldstein, B. Langford, J. Cash, N. R. P. Harris, L. Brown, R. Rinnan, S. Schobesberger, T. Holst, J. E. Mak

predictions during high-temperature periods. This has important implications for air quality and climate modeling in a warming world.

1. Introduction

Isoprene is a reactive volatile organic compound (VOC) emitted in large quantities by terrestrial vegetation. It has the largest emission rate of any non-methane VOC, with total annual isoprene emissions estimated at ∼300–800 Tg a^{-1} (Guenther et al., 2012). Emission rates differ among plant species and are sensitive to environmental conditions including temperature and sunlight (Guenther et al., 1993), soil moisture (Potosnak et al., 2014), and canopy environment properties like leaf area and leaf age (Alves et al., 2016, 2018; Chen et al., 2018; Goldstein et al., 1998; Wu et al., 2016), resulting significant emission variability across a large range of spatial and temporal scales. As a precursor to ozone (O_3), carbon monoxide (CO), formaldehyde (CH_2O), and secondary organic aerosols (SOA), as well as a major sink for the hydroxyl (OH) radical (the primary oxidizing agent in the troposphere), isoprene has a large impact on global atmospheric chemistry and climate processes (Claeys et al., 2004; Sprengnether et al., 2002; Trainer et al., 1987). Accurate estimates of isoprene emissions are required in atmospheric chemistry and climate models to minimize uncertainties in trace gas and aerosol concentrations, greenhouse gas lifetimes (Pike & Young, 2009), radiation budgets, and cloud and aerosol processes (Palmer et al., 2022; Stanton & Tandon, 2023).

Temperature and sunlight are the primary drivers of short-term isoprene emission variability due to the coupling of isoprene emissions with photosynthesis (Guenther et al., 1993). The temperature response of isoprene emissions can be modeled as an exponential increase with temperature up to an optimum value, beyond which further increases in temperature lead to a reduction in emissions (Guenther et al., 2006). Previous studies have found that the magnitude of this optimum as well as the temperature at which it occurs depend on past temperatures on timescales from one day to several weeks (Geron et al., 2000; Hanson & Sharkey, 2001; Monson et al., 1994; Pétron et al., 2001), possibly due to changes in the production of the isoprene substrate dimethylallyl pyrophosphate (DMAPP) or the activity of the isoprene synthase enzyme (Fall & Wildermuth, 1998). In this way, emissions exhibit a thermal hysteresis effect where plants acclimated to higher average temperatures will have a larger emission peak at a higher temperature than plants acclimated to lower temperatures. In isoprene emission models, the temperature response can be represented as a dimensionless activity factor commonly denoted by γ_T which scales vegetation-specific emission factors up or down depending on temperature (Guenther et al., 2006, 2012).

While there has been much success in modeling instantaneous temperature-driven isoprene emission variability (e.g., Situ et al., 2014), substantial uncertainties remain. Recent studies have found that γ_T as it is implemented in the widely used Model of Emissions of Gases and Aerosols from Nature (MEGAN) (Guenther et al., 2006) may be underestimating the temperature sensitivity of isoprene emissions for some vegetation types; isoprene emission studies have historically focused on closed-canopy forest environments, so the variable performance of models across different ecosystems may partially reflect this bias (Guenther et al., 2020). Elevated temperature sensitivity of isoprene emissions has been reported in several environments including high-latitude tundra (Angot et al., 2020; Holst et al., 2010; Kramshøj et al., 2016; Seco et al., 2020, 2022; Tang et al., 2016; Tiiva et al., 2008), boreal wetland vegetation (Vettikkat et al., 2023), Australian *Eucalyptus* trees (Emmerson et al., 2020), and tropical rainforest in the Amazon basin (DiMaria et al., 2023) and Borneo (Langford et al., 2010). This underestimated temperature sensitivity can lead to low biases in isoprene emission estimates during high-temperature periods, which has important implications for air quality modeling during heatwaves (Emmerson et al., 2020; Ferracci, Bolas, et al., 2020; Ferracci, Harris, et al., 2020) and in a warming climate, particularly at high-latitude sites due to rapidly increasing temperatures in that region compared to the rest of the world (England et al., 2021).

In a previous study, DiMaria et al. (2023) found that by optimizing the parameterization of the temperature response function γ_T using eddy covariance isoprene flux observations within a Metropolis-Hastings Markov Chain Monte Carlo (MHMCMC) data assimilation framework, the temporal variability of MEGAN isoprene emissions at an Amazonian field site agreed more closely with the observations. That same study found lower temperature sensitivity at a UK field site, adding to a growing body of evidence that the temperature sensitivity of isoprene emissions varies among ecosystems. Because that study reported results for just two sites, broader conclusions about ecosystem-scale variability in the temperature response could not be drawn. A recent meta-analysis of more than 40-year of plant monoterpene emissions has found that the temperature sensitivity varies with plant functional type and that these variations can be modeled by re-parameterizing MEGAN (Bourtsoukidis et al., 2024). However, because that study primarily focused on the light-independent fraction of monoterpene emissions whose temperature response is represented by a simple exponential function in MEGAN, their conclusions cannot be directly translated to isoprene which has a more complex temperature response function. Other studies using different optimization methodologies have also improved the modeled temperature sensitivity of isoprene emissions for a variety of vegetation types including palm oil plantations (Misztal et al., 2011), tropical rainforest (Langford et al., 2010), high-latitude tundra and wetlands (Seco et al., 2022; Vettikkat et al., 2023), and *Eucalyptus* trees (Emmerson et al., 2020). However, differences in methodology, including but not limited to the formulation of the modeled temperature response, the choice of normalization temperature, the use of either air or leaf temperature to drive modeled temperature sensitivity, and the use of canopy models of varying degrees of complexity, make direct comparisons between existing studies challenging. Furthermore, most of these existing studies did not directly optimize the modeled thermal hysteresis effect. Recent studies have shown that this effect may play an important role in controlling the enhanced temperature sensitivity observed in high-latitude vegetation, particularly sedges (H. Wang et al., 2024a, 2024b). Similar enhancements were also seen for sedges in urban environments (H. Wang, Nagalingam, et al., 2024).

In this study, we build upon the work of DiMaria et al. (2023) and use observations at 11 field sites to measure the isoprene emission temperature response. The sites represent a diverse range of ecosystems including high-latitude and alpine tundra, tropical rainforest, and temperate woodlands. We use an updated data filtering and normalization methodology to derive the emission temperature sensitivity from isoprene flux and concentration measurements which is less sensitive to model errors than the method used by DiMaria et al. (2023). We then apply the same MHMCMC data assimilation methodology from that study to optimize the parameterization of the modeled temperature response $\boldsymbol{\gamma_T}$ at each measurement site to improve model-observation agreement where possible. A consistent methodology is applied to all field sites, allowing for direct comparison of the temperature sensitivity across a wide range of ecosystems. Special attention is given to the parameterization of the thermal hysteresis effect. The overall aim of this study is to quantify the variability of the temperature response across ecosystems and obtain an optimized parameterization for $\boldsymbol{\gamma_T}$ at each site which best reflects the observations. The long-term goal of this work is to develop an ecosystem-specific parameterization of $\boldsymbol{\gamma_T}$ that can be used in global isoprene emission models.

2. Methods

2.1. Field Sites and Measurement Descriptions

The locations of the field sites are shown in Figure 1, and the basic properties of the data sets are presented in Table 1. In addition to isoprene fluxes and concentrations, meteorological measurements including temperature (T), photosynthetic photon flux density (PPFD), soil water content (SWC), leaf area index (LAI), wind speed (WS), and wind direction (WD) were also used, though not all quantities were available for every site. More information about each data set, including measurement site characteristics, is available in Text S1 in Supporting Information S1. Note that the STM data set was previously used by DiMaria et al. (2023); we retain it here only for the purpose of validating our updated data filtering and normalization methodology, described in Section 2.3.

2.2. Modeling the Isoprene Emission Temperature Response With γ_T

In the MEGAN model, the sensitivity of isoprene emissions to temperature can be represented by the dimensionless function γ_T (Guenther et al., 2006), given by

$$\gamma_T = E_{Opt}\left[\frac{\mathrm{C_{T2}}\exp(\mathrm{C_{T1}}x)}{(\mathrm{C_{T2}} - \mathrm{C_{T1}}(1 - \exp(\mathrm{C_{T2}}x)))}\right], \tag{1}$$

where x is a temperature-dependent variable given by

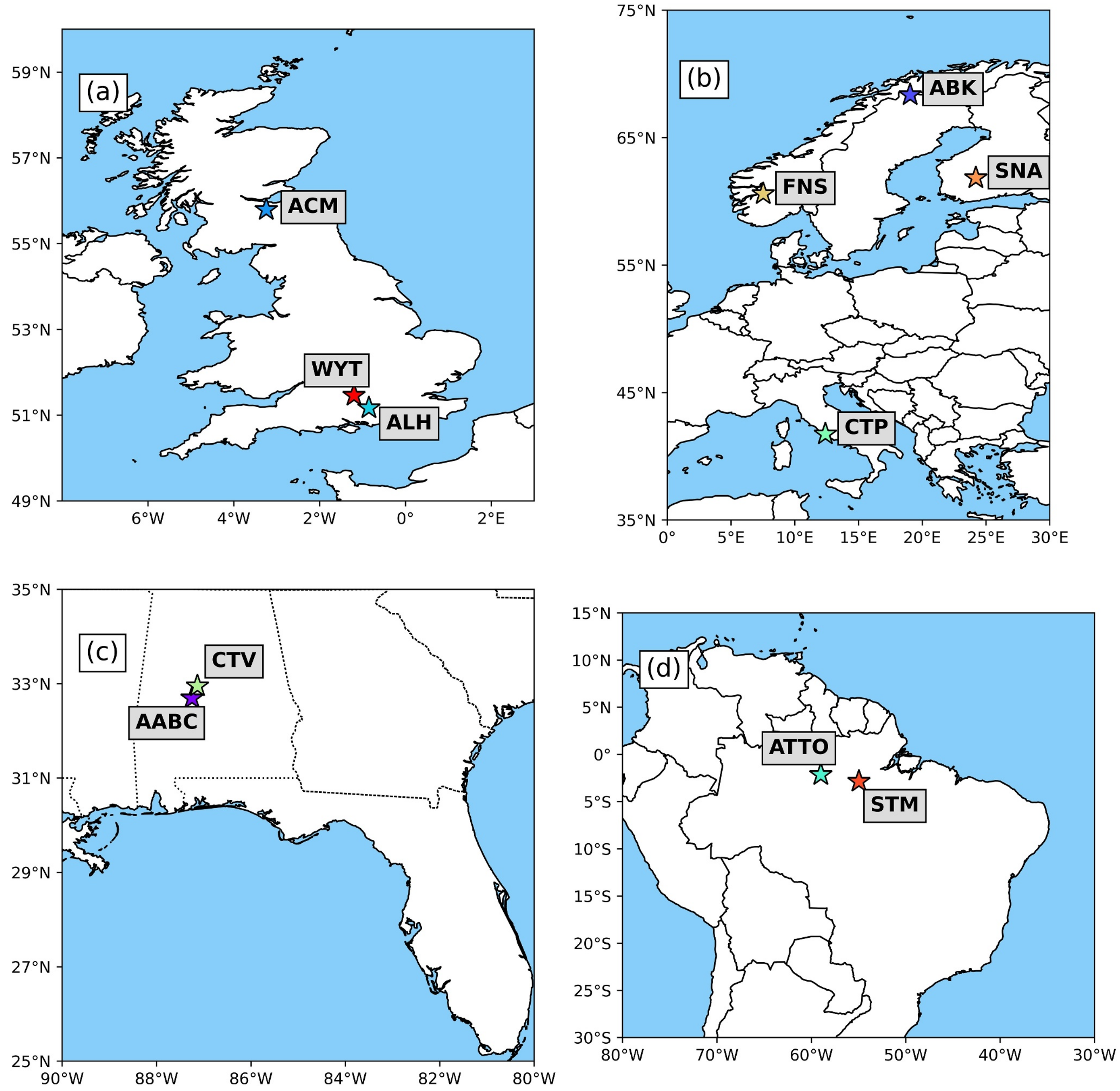

Figure 1. Location of field sites used in this study. Site descriptions are given in Table 1 and in Text S1 in Supporting Information S1. (a) Three field sites (ALH, WYT, and ACM) are on the island of Great Britain. (b) Four field sites are in continental Europe, including one (CTP) in Italy and three (ABK, FNS, and SNA) in Fennoscandia. (c) Two field sites (AABC and CTV) are in Alabama in the Southeastern United States. (d) Two field sites (ATTO and STM) are in the Brazilian Amazon. The STM and WYT sites were also used in DiMaria et al. (2023).

$$x = \left[\frac{\frac{1}{T_{Opt}} - \frac{1}{T}}{R} \right], \tag{2}$$

R is the ideal gas constant (0.00831 kJ K^{-1} mol^{-1}), T_{Opt} is the peak emission temperature given by

$$T_{Opt} = T_{\text{MAX}} + [K_1(T_{24} - 297)], \tag{3}$$

Table 1
Field Site and Data Set Descriptions

Site	Location	Vegetation description	Time period[a]	Measurement type	Ancillary data	References
AABC	Alabama Aquatic Biodiversity Center, AL, USA (32.695°N, 87.249°W)	Mixed temperate forest	2 Jun–14 Jul 2013	Concentration	T PPFD WS WD LAI SWC	Su et al. (2016) Nagori et al. (2019)
ABK	Stordalen mire complex, near Abisko, Sweden (68.356°N, 19.045°E)	High-latitude tundra	7–31 Jul 2018	Flux	T[b] PPFD	Seco et al. (2022)
ACM	Auchencorth Moss, near Penicuik, Scotland, UK (55.792°N, 3.242°W)	Transitional lowland bog	1 Jun–21 Jul 2015	Flux	T PPFD	Langford et al. (2022)
ALH	Alice Holt Forest, Hampshire, England, UK (51.17°, 0.85°W)	Oak-dominated deciduous forest	15 Jun–16 Aug 2005	Flux	T PPFD LAI	Langford et al. (2017)
ATTO	Amazon Tall Tower Observatory, Amazonas, Brazil (2.144°S, 59,000°W)	Tropical rainforest	1–31 Aug 2014	Concentration	T PPFD WS WD	Yáñez-Serrano et al. (2015) Dias-Junior et al. (2014)
CTP	Castelporziano, Lazio, Italy (41.74°N, 12.40°E)	Mediterranean coastal hygrophilous forest	13 Sep–1 Oct 2011	Flux	T PPFD LAI	Fares et al. (2013) Langford et al. (2017)
CTV	SEARCH flux tower, Brent, Alabama, USA (32.95°N, 87.134°W)	Mixed temperate forest/agricultural	2 Jun–14 Jul 2013	Concentration	T PPFD WS WD	Hidy et al. (2014) Xiong et al. (2015)
FNS	Hardangarvidda plateau, near Finse, Norway (60.594°N, 7.527°E)	Oroarctic (alpine) tundra	1 Jul–15 Sep 2019	Flux	T[b] PPFD	Seco et al. (2022)
SNA	Siikaneva 1 site, near Hyytiälä Forestry Field Station, Finland (61.833°N, 24.193°E)	Oligotrophic fen (boreal wetland)	19 May–28 Jun 2021	Flux	T PPFD LAI	Vettikkat et al. (2023)
STM	AmeriFlux site BR-Sa1, near Santarém, Pará, Brazil (2.857°S, 54.959°W)	Tropical rainforest	1–16 Jun 2014	Flux	T PPFD	Sarkar et al. (2020, 2022)
WYT	Wytham Woods, Oxfordshire, England, UK (51.46°N, 1.20°W)	Oak-dominated deciduous forest	25 May 2018–15 Oct 2022	Concentration	T PPFD SWC LAI WS WD	Ferracci, Bolas, et al. (2020), Ferracci, Harris, et al. (2020) Brown et al. (2020) Environmental Change Network (EC) http://www.ecn.ac.uk/

[a] In some cases longer time series were available, but we used a smaller subset of the data to limit variability associated with seasonal changes in leaf area, leaf age, and soil moisture. [b] Both air temperature and vegetation surface temperature measurements were available at these sites.

Table 2
A Priori γ_T Parameterization Used in This Study

Parameter	Value	Description
C_{EO}	1.75	Normalization factor
T_{MAX}	313 K	Peak emission temperature
C_{T1}	80 kJ mol^{-1}	Fitting parameter
C_{T2}	200 kJ mol^{-1}	Fitting parameter
K_1	0.6	Sensitivity of T_{Opt} to T_{24}
K_2	0.08	Sensitivity of E_{Opt} to T_{24}

and E_{Opt} is the optimum emission point given by

$$E_{Opt} = \mathrm{C_{EO}} \times \exp[K_2(T_{24} - 297)]. \tag{4}$$

The parameters $\mathrm{C_{T1}}$ and $\mathrm{C_{T2}}$ are empirical fitting parameters which control the width of the γ_T function along the temperature axis, while $\mathrm{T_{MAX}}$ is the temperature at which emissions are maximized. The T_{24} term represents the average temperature of the past 24 hr Equations 3 and 4 describe the thermal hysteresis effect, in which the temperature of peak emissions T_{Opt} and magnitude of peak emissions E_{Opt} change based on past temperatures. The empirical parameters K_1 and K_2 set the strength of this hysteresis effect and are based on a relatively small number of experimental studies (Geron et al., 2000; Hanson & Sharkey, 2001; Monson et al., 1994; Pétron et al., 2001). The $\mathrm{C_{EO}}$ parameter is a normalization factor that controls the magnitude of the emissions (Guenther et al., 2012).

Note that the thermal hysteresis effect has been observed over a range of time scales, and different implementations of the γ_T algorithm have accounted for this variability over 15-day (e.g., Guenther et al., 1999) and 10-day time scales (e.g., Guenther et al., 2006) in addition to 24-hr time scales through the use of additional parameters in Equations 3 and 4 or by using different numerical values of K_1 and K_2. We focus on the 24-hr time scale to ensure consistency with the previous work of DiMaria et al. (2023). Sensitivity tests showed that optimizing the parameterization of the thermal hysteresis effect in γ_T across multiple time scales simultaneously (e.g., by including both T_{24} and T_{240}) was not feasible because the observation uncertainties were too large to constrain this relatively small additional source of variability. However, it is likely that longer-term effects play a role for at least one data set in Table 1. At the SNA site, Vettikkat et al. (2023) found that isoprene emissions were elevated for several days after a short period of anomalously hot weather. This provides direct evidence that thermal hysteresis impacts isoprene emissions at this site on time scales longer than 24 hr, but optimizing this longer-term effect is beyond the scope of this study.

We use the Parameterized Canopy Environment Emission Activity (PCEEA) implementation of γ_T. In this version, the empirical parameter values are based on a canopy physics simulation for warm broadleaf forests (Guenther et al., 2006). Table 2 shows the PCEEA parameter values used in our study. Canopy physics processes, including the relationship between air temperature and vegetation surface temperature, are implicitly contained in the empirical parameterization of γ_T. The uncertainties associated with our use of the PCEEA implementation have been discussed in DiMaria et al. (2023) and are discussed in Section 4.3.2. While full canopy-physics versions of MEGAN exist (e.g., MEGAN3 (Guenther et al., 2020)), parameterizations like the PCEEA are more easily integrated in global atmospheric chemistry models because they require fewer driving variables and have lower computational costs (Silva et al., 2020). Optimized versions of these simplified parameterizations can therefore be more readily applied in global models.

Note that γ_T is not intended to model secondary temperature-related impacts on isoprene emissions during times of drought stress. In particular, isoprene emissions have been observed to increase under conditions of moderate drought (Otu-Larbi et al., 2020; Seco et al., 2015), and this effect is thought to be due to increased leaf temperature due to a reduction in evapotranspiration from the leaf surface (Potosnak et al., 2014). While the empirical parameters in γ_T could in principle be tuned during times of drought to capture this behavior, this would be inappropriate as it ignores the underlying mechanistic drivers. We therefore limit our analysis in this study to non-drought conditions to ensure we are not misattributing drought effects to errors in the γ_T parameterization.

2.3. Deriving γ_T From Observations

The data sets described in Section 2.1 consist of isoprene flux or mixing ratio measurement time series, along with ancillary meteorological observations including temperature, sunlight, and in some cases soil moisture, windspeed, WD, and leaf area index. To obtain the temperature response from these data, other sources of emission variability must be filtered out. This filtering process is briefly described in Section 2.3.1. Additional details are available in Text S2 in Supporting Information S1.

Table 3
Measurement Filter Characteristics and Observed Q_{10} Values

	Filter thresholds/Bands					
Site	PPFD (μmol/m^2/s)	LAI (m^2/m^2)	WS (m/s)	WD (°)	$N_{Obs}/N_{Filtered}$	Q_{10}
AABC	>800	---	1.199–2.344	105.54–286.19	557/20	4.83 ± 1.09
ABK	>1,500	---	---	---	1,488/53	11.16 ± 1.36 (air) 11.17 ± 1.94 (leaf)
ACM	>1,200	---	---	---	168/15	15.77 ± 8.23
ALH	>650	>4.8	---	---	1,156/59	5.81 ± 1.04
ATTO	>1,640	---	1.42–3.58	73.9–224.4	293/21	2.62 ± 0.88
CTP	>3,000	>4.8	---	---	187/26	3.47 ± 1.66
CTV	>800	---	0.586–2.913	77.31–189.4	426/18	2.92 ± 0.52
FNS	>1,500	---	---	---	3,648/71	2.68 ± 0.49 (air) 2.21 ± 0.34 (leaf)
SNA	>1,500	0.2–0.55[a]	---	---	543/41	4.88 ± 0.79[b]
WYT[c]	>1,300	3.2	0.8787–2.575	140.6–230.6	10,308/58 (66 during drought conditions[c])	7.95 ± 0.91 (4.01 ± 0.32 during drought conditions[c])

Note. Entries containing three dashes ("---") indicate that data was not available. [a]Isoprene fluxes were normalized by γ_{LAI} due to large monotonic increase in LAI throughout the measurement time series at SNA. [b]Our Q_{10} at SNA is different than in Vettikkat et al. (2023) due to our higher PFFD cutoff, normalization by LAI, and inclusion of heat-stress affected data which were omitted from the calculation of Q_{10} in that study. [c]The WYT data were additionally filtered for soil water content (SWC) > 22% to exclude drought conditions.

Once the measurements have been filtered, they must be normalized such that they can be directly compared with the dimensionless temperature response function γ_T. This normalization process, which is described in Section 2.3.2, ensures that we can quantitatively compare the observed and modeled temperature sensitivity without being affected by uncertainties in the magnitude of modeled emissions, which are sensitive to errors in vegetation-specific basal emission factors (Batista et al., 2019; Guenther et al., 1993, 1995; Li et al., 2021).

2.3.1. Observation Filtering

To extract the temperature sensitivity from isoprene flux observations, it is necessary to account for other sources of emission variability including sunlight, leaf area, and soil moisture. The use of isoprene concentration measurements instead of fluxes requires additional filtering, as isoprene concentrations will depend not only on emission rates but also on chemistry and transport processes in the atmosphere (Ferracci, Bolas, et al., 2020; Ferracci, Harris, et al., 2020). We filter the observations to account for isoprene variability due to PPFD, SWC, LAI, WS, and WD. Table 3 shows the filtering thresholds used at each measurement site. Briefly, filtering for measurements with high PPFD values eliminates sunlight-drive isoprene emission variability and also minimizes variability in photochemical loss rates and vertical mixing. Similarly, filtering based on LAI and SWC limits isoprene emission variability due to changes in leaf area and drought stress. Accounting for WS and WD minimizes variability in atmospheric dispersion rates, which is necessary when using isoprene concentration measurements instead of flux measurements. A detailed description of the data filtering process is available in Text S2 in Supporting Information S1, which includes justifications for the thresholds presented in Table 3 and a consideration of potential sources of error (see also the Discussion in Sections 4.3.3 and 4.3.4).

Figures 2 and 3 show the isoprene measurement time series data at each field site (left column), with filtered measurements indicated. Also shown (right column) are the same data plotted against temperature measurements. At the SNA site (Figures 3g and 3h), the isoprene fluxes have been normalized by LAI using the MEGAN leaf area activity factor,

$$\gamma_{LAI} = \frac{0.49LAI}{\sqrt{1 + 0.2LAI^2}}, \tag{5}$$

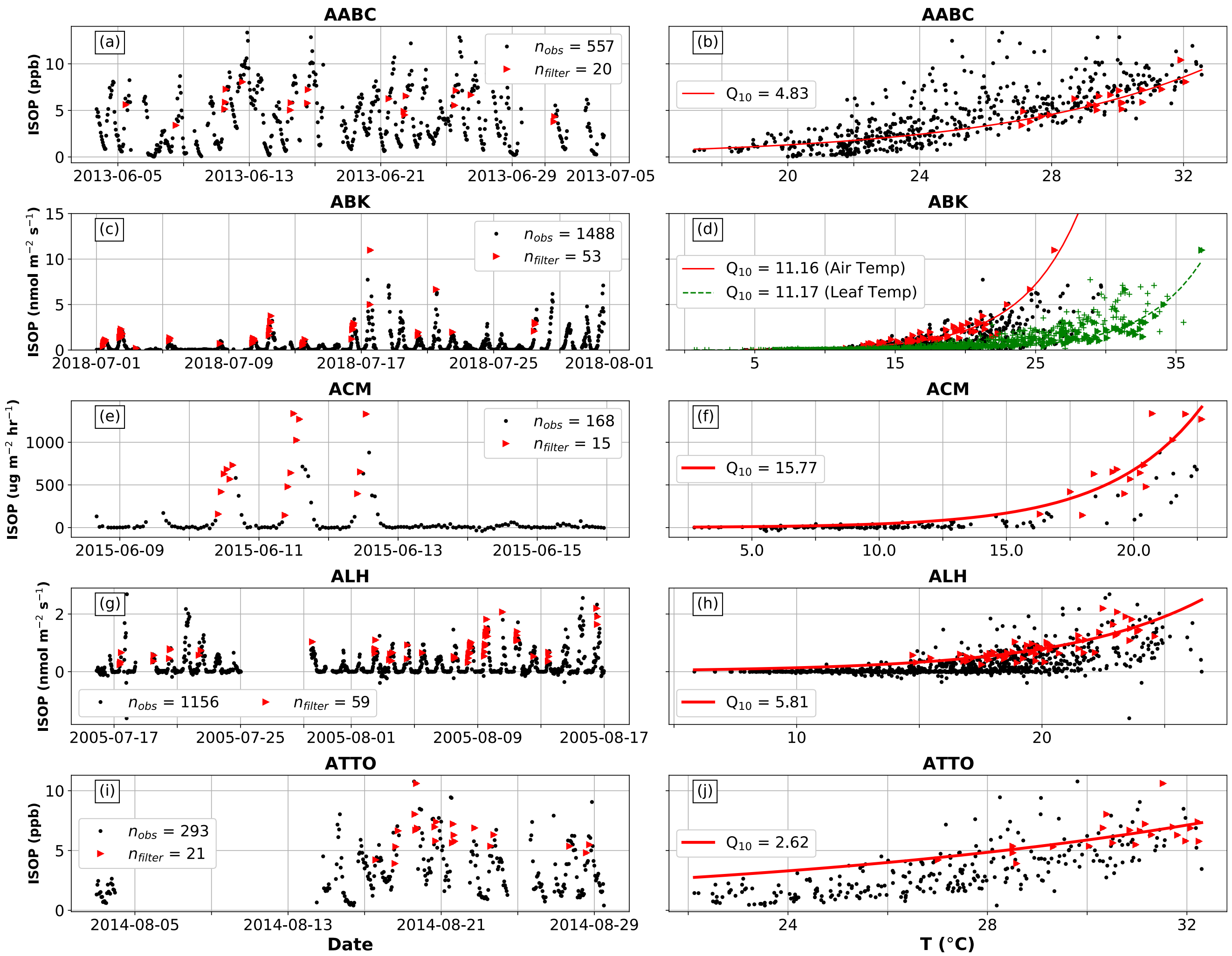

Figure 2. Raw (black) and filtered (red) isoprene measurement time series at field sites AABC, ABK, ACM, ALH, and ATTO (panels a, c, e, g, i). Raw (black dots) and filtered (red triangles) isoprene measurements plotted against temperature at the same field sites (panels b, d, f, h, j). The function fits in the right column are calculated with Equation 6. For larger versions of these panels, please refer to Figures S8–S12 in Supporting Information S1. The green data in panel (d) is plotted against leaf temperature (crosses show unfiltered data, triangles show filtered data).

where LAI is the leaf area index (Guenther et al., 2006). Larger versions of these plots are available in the Supporting Information (Figures S7–S16 in Supporting Information S1). An exponential fit to the filtered data as a function of temperature is shown, described by

$$ISOP = F_0 \times Q_{10}^{\left(\frac{T-T_0}{10}\right)}, \qquad (6)$$

where F_0 is the value of $ISOP$ at a chosen normalization temperature T_0 (in this case, equal to the mean temperature of each data set) and Q_{10} is equal to the fractional change in $ISOP$ for a 10° change in temperature. This approach is based on the method of Seco et al. (2022). Q_{10} is therefore a measure of the sensitivity of $ISOP$ to temperature, and it does not depend on the chosen normalization temperature T_0. The Q_{10} values listed in Table 3 were all calculated using Equation 6, with only the filtered observations included in the calculation.

Note that for two data sets (ABK and FNS), leaf temperature measurements were available in addition to air temperature measurements. Leaf temperatures were generally higher than air temperatures, but the measured temperature sensitivity Q_{10} was largely unaffected by the choice of temperature data (the differences in Q_{10} values in Figures 2d and 3f are not statistically significant given the errors on Q_{10}). Other studies have found that this is

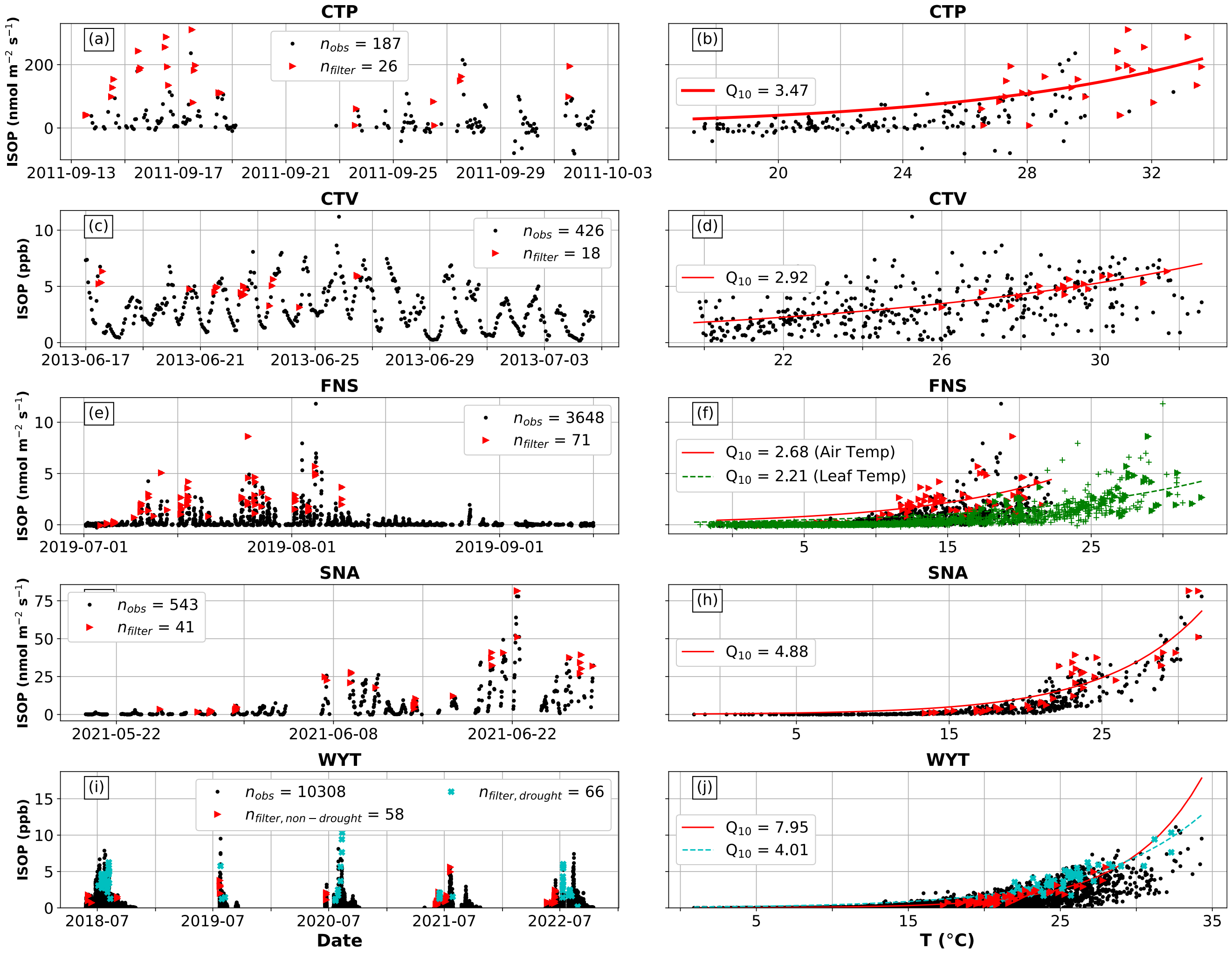

Figure 3. Raw (black) and filtered (red) isoprene measurement time series at field sites CTP, CTV, FNS, SNA, and WYT (panels a, c, e, g, i). Raw (black dots) and filtered (red triangles) isoprene measurements plotted against temperature at the same field sites (panels b, d, f, h, j). The function fits in the right column are calculated with Equation 6. For larger versions of these panels, please refer to Figures S13–S17 in Supporting Information S1. The green data in panel (f) is plotted against leaf temperature (crosses show unfiltered data, triangles show filtered data). The blue X symbols in panels (i)–(j) were impacted by drought stress and were omitted from subsequent analyses.

not always the case. For example, Seco et al. (2020) found a strong dependence of Q_{10} on the choice of air temperature/leaf temperature data at a wetland site located only a few hundred meters away from our high-latitude tundra site at Abisko, illustrating that the importance of leaf temperature measurements varies across ecosystems. Note also that the impact of drought stress on temperature sensitivity is clearly apparent at WYT in Figures 3i and 3j; emissions are generally higher during drought periods, but the measured sensitivity of emissions to temperature is actually lower. While not the focus of this paper, there is clearly a relationship between drought and isoprene emission temperature sensitivity that warrants further investigation.

2.3.2. Normalization

The measurements shown in Figures 2 and 3 are expressed in units of isoprene fluxes or concentrations, while γ_T is a dimensionless scaling factor. To allow for a direct comparison between the observations and γ_T, we normalize both quantities such that they are equal to 1 at the mean temperature of each data set. This allows for a direct comparison of the measured and modeled sensitivity of emissions to temperature (i.e., the change in emissions for a given change in temperature) as quantified by the Q_{10} term in Figures 2 and 3. Note that the temperature sensitivity as quantified by Q_{10} does not depend on normalization, since it only measures the relative change in

Algorithm 1: Sampling P(x|y) using adaptive MHMCMC

```
1.  $\mathbf{x}_i = \mathbf{x}_a$                                  (initialize model parameters to a priori values)
2.  FOR i < N:
3.      $\mathbf{x}_{i+1} = \mathbf{x}_i + \Delta\mathbf{x}$                 (perturb model parameters by $\Delta\mathbf{x}$)
4.      $\mathbf{H}(\mathbf{x}_i) = \mathbf{H}_i,\ \ \mathbf{H}(\mathbf{x}_{i+1}) = \mathbf{H}_{i+1}$   (run model with both sets of parameters)
5.      IF $\frac{P(\mathbf{x}_{i+1}|\mathbf{y})}{P(\mathbf{x}_i|\mathbf{y})} > U \in [0,1]$:        (compare probability of $\mathbf{x}_{i+1}$ and $\mathbf{x}_i$)
6.              RETURN $\mathbf{x}_{i+1}$                      (accept new parameters $\mathbf{x}_{i+1}$)
7.      ELSE:
8.              RETURN $\mathbf{x}_i$                          (reject new parameters)
9.      IF $i\%n_{step} = 0$:                        (adjust step size every $n_{step}$ iterations)
10.             $\Delta\mathbf{x} = \Delta\mathbf{x} + \boldsymbol{\delta}$
```

Figure 4. Metropolis-Hastings Markov Chain Monte Carlo data assimilation algorithm. Steps 2 to 10 are repeated for a user-defined number of iterations *N*. In this study we use $N = 40{,}000$. The step size $\Delta\mathbf{x}$ is adjusted every n_{step} iterations to ensure a sample acceptance rate of between 23% and 44%.

emissions for a 10-degree change in temperature. The normalized observations are compared to γ_T in Figure 5 for each data set.

This normalization method effectively gives us an "observed" γ_T from the filtered time series observations, consistent with the approach used in other isoprene flux studies (e.g., Seco et al., 2022; Vettikkat et al., 2023; H. Wang et al., 2024b). The method previously used by DiMaria et al. (2023) to derive an "observed" γ_T relied on calculating other MEGAN activity factors such as γ_{PAR} (the sunlight response) and γ_{LAI} (the leaf area response). Each of these activity factors is subject to uncertainties, and while the impact of these uncertainties was largely mitigated in DiMaria et al. (2023) by filtering out non-temperature sources of emission variability, our current method circumvents this problem entirely. This is particularly important given that possible errors in the sunlight response γ_{PAR} have already been reported for one of the data sets used here (Langford et al., 2022). Our current method is sensitive only to errors in the isoprene observations and in the quality of data filtering, not to errors in any additional modeled quantities. The only exception is the SNA data set, where we had to use γ_{LAI} to normalize the isoprene flux measurements as described in Section 2.3.1.

2.4. Optimizing Model Parameters

Our goal is to optimize the γ_T parameters independently at each of the measurement sites to improve model performance. Excluding the C_{EO} parameter because it has no impact on the normalized temperature response, there are 31 unique combinations of the remaining 5 γ_T parameters (T_{MAX}, C_{T1}, C_{T2}, K_1, and K_2). Only those parameters included in a given combination are optimized, while the remaining parameters are fixed to their a priori values from Table 2 (e.g., optimizing T_{MAX} while leaving C_{T1}, C_{T2}, K_1, and K_2 fixed). At each site, we attempt to optimize all 31 parameter combinations using only the observations from that site. The sensitivity of γ_T to the various empirical parameters is highly variable and depends on temperature, with most parameters having a larger impact on γ_T at higher temperatures (DiMaria et al., 2023). As a result, some combinations of parameters are easier to constrain with observations than others. Furthermore, because each data set has a different measurement error, parameter combinations that can be reliably constrained at one measurement site may not be constrained at a different site.

One structural limitation of our analysis is the assumption that even though the parameter values may be incorrect, γ_T is still the correct model of the isoprene emission temperature response (i.e., the functional form of γ_T adequately describes temperature response). While obtaining a new functional form for γ_T is beyond the scope of this study, we attempt to deal with this limitation by using two separate optimization algorithms to constrain the γ_T parameters. We first use a Levenberg-Marquardt (LM) non-linear least squares curve-fitting algorithm (see Text S3 in Supporting Information S1) to optimize all parameter–dataset combinations, without accounting for observation errors. The only purpose of this experiment is to determine whether γ_T can in principle be re-parameterized to capture the observed temperature response at each field site. This accounts for the possibility that the functional form of γ_T may be mischaracterized for some vegetation types. If γ_T cannot be fit to the observations at a particular field site for any parameter values even with zero observation error, it is possible that the temperature response may not be appropriately characterized at that site. In such cases it would not be sensible to proceed with the MHMCMC optimization. These experiments are presented in Text S4 in Supporting Information S1.

For each promising configuration identified with the LM algorithm, we then use a MHMCMC algorithm which properly accounts for the observation errors to optimize the model parameters (see Section 2.4.1). The MHMCMC approach provides robust estimates of the posterior parameter probability distribution which considers the sensitivity of γ_T to the parameters and the observation error, while also revealing emergent correlations between free parameters.

2.4.1. MHMCMC Algorithm

The MHMCMC method uses Bayesian inference to combine information from models and observations in a statistically consistent way (Haario et al., 2001). This technique has been applied in ecosystem modeling contexts to constrain empirical model parameters (e.g., Bloom et al., 2015; Bloom et al., 2020; Xu et al., 2006; Ziehn et al., 2012). Starting from Bayes' Theorem, for a vector **x** containing the model parameters, we can define the posterior probability density function of **x** given a set of observational constraints **y** as

$$P(\mathbf{x}|\mathbf{y}) \propto P(\mathbf{x})\,P(\mathbf{y}|\mathbf{x}) \tag{7}$$

where $P(\mathbf{x})$ is the a priori probability distribution of **x** and $P(\mathbf{y}|\mathbf{x})$ is the model likelihood function (i.e., the likelihood of a set of observations **y** given model parameters **x**). Assuming Gaussian error statistics and no covariance between observation errors, we can define a model likelihood function as

$$P(\mathbf{y}|\mathbf{x}) = \exp\left(-0.5\sum_{n=1}^{n_{obs}}\frac{\left(H_n(\mathbf{x}) - y_n\right)^2}{\sigma_n^2}\right) \tag{8}$$

where n_{obs} is the total number of observations, y_n is the nth observation, $H_{\mathrm{n}}(x)$ is the corresponding model state (i.e., the value of γ_T given a particular set of model parameters), and σ_n^2 is the observation variance.

We follow DiMaria et al. (2023) and assume a non-informative uniform $P(\mathbf{x})$ for all model parameters such that $P(\mathbf{x})$ = constant for all $\mathbf{x} \in [\mathbf{x}_{\min}, \mathbf{x}_{\max}]$ and $P(\mathbf{x}) = 0$ elsewhere. The values of $\mathrm{x}_{\min}$ and $\mathrm{x}_{\max}$ were set to 0.1 and 10 times the prior parameter values shown in Table 2. The use of a non-informative prior with a large range allows the parameter optimization to be more strongly influenced by the observations, instead of being pulled toward the a priori values. This is desirable given the large spread in γ_T parameter values reported in previous studies. For example, Emmerson et al. (2020) measured a five-fold increase in the C_{T2} for *Eucalypt* species under certain growing conditions. Seco et al. (2022) similarly measured large increases in several γ_T parameters, while other studies have found smaller but still significant differences on the order of 50%–100% between the a priori MEGAN predictions and the fitted γ_T parameters (e.g., Langford et al., 2010; Misztal et al., 2011; Wilkinson et al., 2006).

To ensure equal sampling probability across multiple orders of magnitude for the parameters, **x** is log-transformed in the Bayesian inference step of the MHMCMC algorithm, such that $P(\mathbf{x})$ is effectively treated as a log-uniform distribution by the sampling algorithm. With these constraints, the posterior parameter probability $P(\mathbf{x}|\mathbf{y})$ for all $\mathbf{x} \in [\mathbf{x}_{\min}, \mathbf{x}_{\max}]$ is simply proportional to the model likelihood function $P(\mathbf{y}|\mathbf{x})$ given by Equation 8. Maximizing this probability gives us an error-weighted fit of the parameters to the observations, along with their probability distributions.

Because $P(\mathbf{x}|\mathbf{y})$ is proportional to $P(\mathbf{x})P(\mathbf{y}|\mathbf{x})$, we can directly sample the posterior parameter probability distribution (Equation 7) using the model likelihood function (Equation 8). This sampling is done using the adaptive MHMCMC algorithm of Haario et al. (2001), based on the approach of Bloom et al. (2020) and using a MATLAB program developed by Yang et al. (2021, 2022). The algorithm is summarized in Figure 4 below. In Figure 4, $\mathbf{x}_i$ is the ith iteration of the parameter vector **x**, $\mathbf{x}_a$ is the a priori parameter vector, $\Delta\mathbf{x}$ is the parameter perturbation, N is the total number of iterations (4×10^4 in our experiments), $\mathbf{H}(\mathbf{x_i})$ is the model calculated using parameters $\mathbf{x_i}$, $P(\mathbf{x_i}|\boldsymbol{y})$ is the parameter probability calculated using Equation 8, U is a uniform distribution, n_{step} is the perturbation

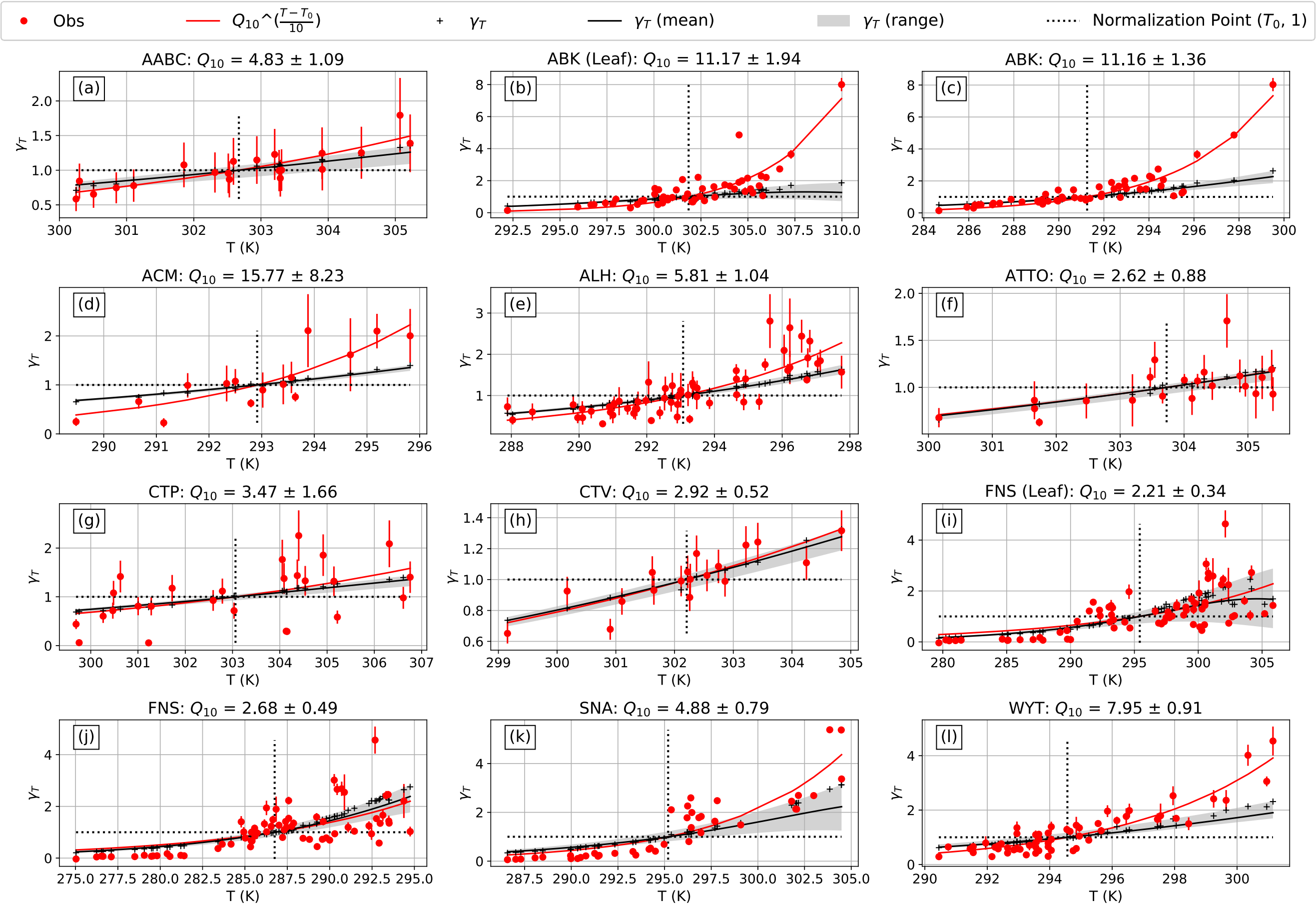

Figure 5. Normalized filtered isoprene measurements (red circles) compared with a priori parameterization of γ_T (black) as a function of air temperature based on the parameters in Table 2 at each measurement site (panels a, c, d, e, f, g, h, j, k, l). Panels b and i show the same information plotted against measured leaf temperature. The black crosses are the a priori MEGAN predictions using the same T and T_{24} values at which the observations were made, while the black line is calculated continuously as a function of T using the mean value of T_{24}. The red curves show an exponential fit to the observations using Equation 2, which was used to derive the Q_{10} sensitivity metric. The red error bars show the observation errors of the measurements propagated through Equation 6. The shaded gray area represents the range of γ_T values due to changes in the mean 24-hr temperature T24, and therefore illustrates the effect of thermal hysteresis as described by Equations 3 and 4.

step size adjustment frequency or learning rate, $\boldsymbol{\delta}$ is the adjustment to the parameter perturbation $\Delta\mathbf{x}$, and % is the modulo operator which returns the remainder of an integer division operation. The length of the parameter vector $\mathbf{x}$ varies from 1–5 depending on how many parameters are being optimized.

Because only the ratio of probabilities is used in Step 5, $P(\mathbf{x}|\mathbf{y})$ does not need to be normalized and so $P(\mathbf{y})$ can be omitted from Bayes' Theorem. Steps 5–8 of Algorithm 1 ensure that parameter values which maximize the probability in given by Equation 8 are more likely to be accepted; the comparison to a random number U between 0 and 1 ensures that there is always some probability of rejecting more likely parameters, which prevents the algorithm from getting stuck in a local probability maximum (Haario et al., 2001). Following Ziehn et al. (2012), the adjustment $\boldsymbol{\delta}$ to the perturbation $\Delta\mathbf{x}$ is chosen from a proposal distribution every n_{step} = 50 to achieve a parameter acceptance rate between 23%–44%; this allows for sufficient exploration of parameter space while minimizing the required number of iterations. This adjustment is done using the evolving covariance of the samples as in Haario et al. (2001) and Bloom et al. (2020). In all of our experiments, the first half of the samples were then discarded as burn-in, and the remaining half were subsampled by a factor of 20 to reduce correlations between samples, giving a final distribution of 1,000 parameter samples for each experiment.

3. Results

3.1. Observed Temperature Response

Figure 5 shows the normalized measured temperature response compared with the a priori γ_T parameterization for each data set (i.e., the parameterization shown in Table 2). The range in γ_T shown in Figure 5 with the gray shading was calculated using the maximum and minimum observed values of T_{24} during the observation period; as such, this represents the thermal hysteresis effect described by Equations 3 and 4 and not an uncertainty. There is large variability in the measured temperature response across the measurement sites. At the AABC, ATTO , CTV, and CTP measurement sites, the observations are in good agreement with the a priori parameterization of γ_T. The good agreement between the observations and γ_T at the Amazonian ATTO site contrasts strongly with the results at the Amazonian STM site (~460 km East of ATTO) reported by DiMaria et al. (2023) (see Figure S1 in Supporting Information S1). The exponential fit to the observations at the FNS site is in good agreement with the a priori γ_T, but there is a large amount of scatter in the high-temperature measurements at that site (Figure 5j). When using leaf temperature measurements (Figure 5i) instead of air temperature (Figure 5j), much of this scatter is contained within variability of γ_T driven by changes in T_{24}; the larger variability of γ_T in Figure 5i is simply due to the larger variability of leaf temperature compared to air temperature, and this can be seen to a lesser extent at the ABK site (Figures 5b and 5c).

The observations showed a higher sensitivity to temperature than the a priori γ_T at the ABK, ALH, SNA, and WYT measurement sites. In particular, the results imply that γ_T underestimates high-temperature isoprene emissions at these sites. This is consistent with the findings of Seco et al. (2022) at the ABK field site. For SNA, the heightened temperature sensitivity observed here is likely due to the impacts of heat stress reported by Vettikkat et al. (2023). That study found that isoprene emissions at the site were substantially higher for several days after a period of abnormally hot temperatures. Notably, the heightened temperature sensitivity at WYT was not observed at this same measurement site in DiMaria et al. (2023). However, that study relied on a much shorter measurement time series (~3 weeks in May–June 2018) which lacked high-temperature observations where the discrepancies between the model and the observations are apparent. This clearly demonstrates the sensitivity of the optimized γ_T parameterization to the observational constraints and suggests that using relatively small data sets to train the parameterization with MHMCMC may introduce out-of-sample biases if the training data set does not capture a sufficiently wide range of temperatures.

3.2. MHMCMC Optimization

We applied the MHMCMC algorithm to all promising parameter configurations from the LM optimization experiments, as described in Text S4 in the Supporting Information S1 (i.e., configurations where an optimized set of parameters could be found when we ignored measurement errors). As expected, many of the parameter configurations could not be reliably constrained due to the low sensitivity of γ_T to the parameters as well as the impact of observation errors. This was especially true at measurement sites where the a priori γ_T was already in good agreement with the observations. While in principle the MHMCMC optimization should simply return the a priori parameters in such cases, in practice the low sensitivity of γ_T to the parameters means that very precise observations are required to discern the impact of changing any of the parameters unless there are large differences between the model and the observations.

Despite these difficulties, we found that the MHMCMC was able to reliably constrain the K_2 parameter at the ABK, SNA, and WYT sites (Figures 6a–6c, respectively). From Equation 4, K_2 determines how sensitive the peak emission rate E_{Opt} is to changes in T_{24} (the average temperature of the past 24 hr). A larger value of K_2 produces a larger change in the peak emission rate E_{Opt} as a function of T_{24}, which is illustrated in Figure S2 in Supporting Information S1. In all three cases, increasing K_2 had little impact on γ_T at low temperatures but greatly improved model-observation agreement at high temperatures. This is clearly visible in the residuals shown in Figure 6d–6f for each site. The probability distributions of the optimized K_2 values for each site are shown in Figures 6g–6i. Note that parameter histogram is much narrower at the SNA site compared to ABK and WYT; this is a direct consequence of the smaller observation errors at SNA (as reported by Vettikkat et al., 2023) compared to the other two sites. The results shown in Figure 6 are summarized in Table 4.

We have chosen to primarily focus on the optimization of K_2 because it has a clear physical interpretation; namely, an increase in K_2 represents a stronger thermal hysteresis effect as governed by Equation 4. The recent

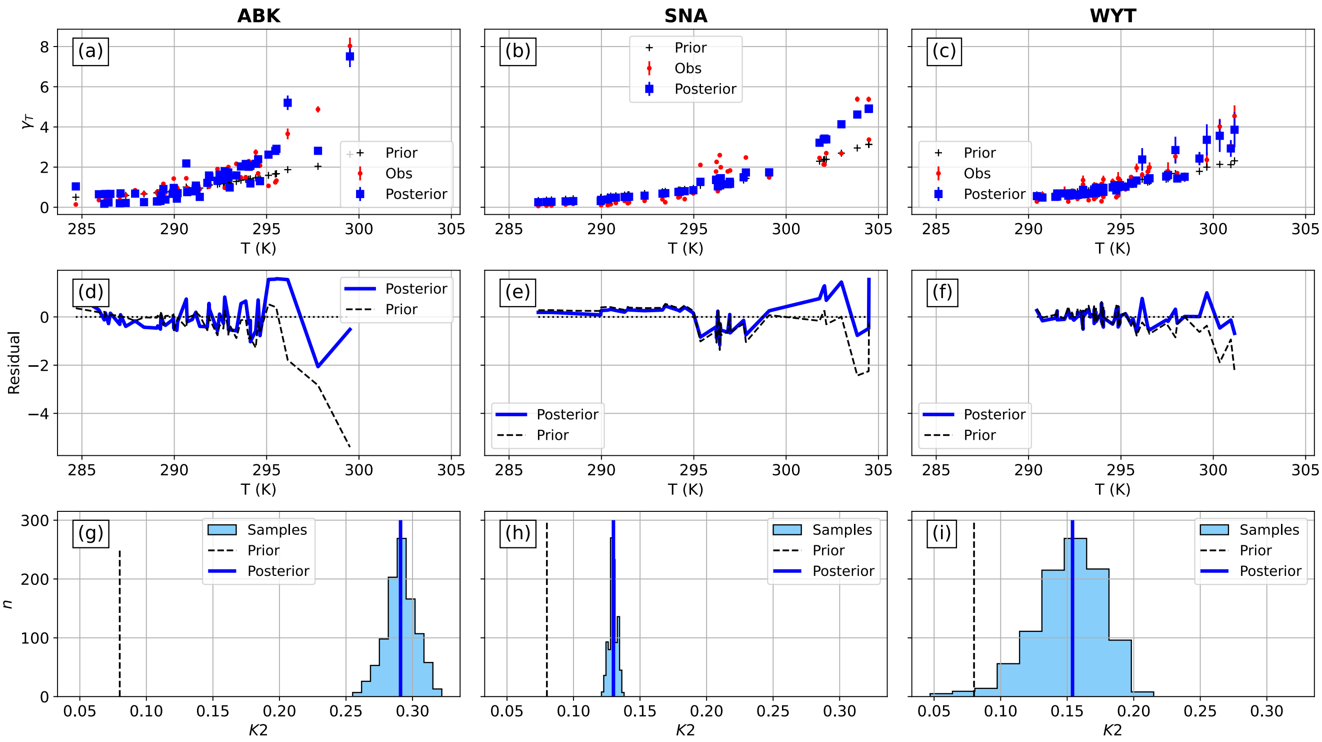

Figure 6. Metropolis-Hastings Markov Chain Monte Carlo optimization results for K_2 parameter at ABK (left), SNA (middle), and WYT (right) measurement sites. The observations, a priori γ_T model, and posterior γ_T model are shown in panels (a)–(c). The residuals are shown in panels (d)–(f). The posterior K_2 distribution is shown in the histograms in panels (g)–(i), with the median value indicated by the solid blue line and the prior value indicated by the dashed black line.

studies of H. Wang et al. (2024a, 2024b), H. Wang, Nagalingam, et al. (2024) suggests that focusing on the parameterization of the thermal hysteresis effect is reasonable. Furthermore, Vettikkat et al. (2023) found increased isoprene emissions after a period of abnormally hot temperatures at SNA, indicating that thermal hysteresis plays an important role at that site.

Figure 7 shows an alternate MHMCMC optimization result at WYT using C_{T1} and C_{T2} as free parameters instead of K_2. As with the K_2 optimization from Figures 6c, 6f, and 6i, the MHMCMC algorithm was able to improve high-temperature model-observation agreement (Figures 7a and 7b) with a similar reduction in the residuals. Figure 7c shows the two-dimensional probability distribution of C_{T1} and C_{T2}, where the color bar indicates the number of parameter samples in each 2D bin. In this case the parameters are not as well constrained as K_2 was in Figure 6i, resulting in larger posterior errors in Figure 7a. The area below the dashed line in Figure 7c is within the allowable range of the C_{T1} and C_{T2} parameters (specifically, $C_{T2} > 20$ and $C_{T1} > 8$); however, the sampling algorithm avoids this region because simultaneously using large values of C_{T1} and small values of C_{T2} leads to large biases between the model and the observations. This illustrates how MHMCMC can reveal correlations between model parameters.

Table 4
Selected Metropolis-Hastings Markov Chain Monte Carlo Optimization Results

Site	Free parameters	Prior residual	Posterior residual	Prior parameters	Posterior parameter median	Posterior parameter StdDev
ABK	K_2	−0.338	−0.025	0.08	0.291	0.011
SNA	K_2	0.247	0.121	0.08	0.130	0.003
WYT	K_2	−0.115	−0.010	0.08	0.154	0.026
WYT	$C_{T1}C_{T2}$[a]	−0.115	−0.006	80 kJ mol^{-1} 200 kJ mol^{-1}	193 kJ mol^{-1} 640 kJ mol^{-1}[a]	60 kJ mol^{-1} 490 kJ mol^{-1}[a]

[a] The posterior C_{T2} distribution is highly skewed (see Figure 7c), with a median of 640 and a mode of 282.

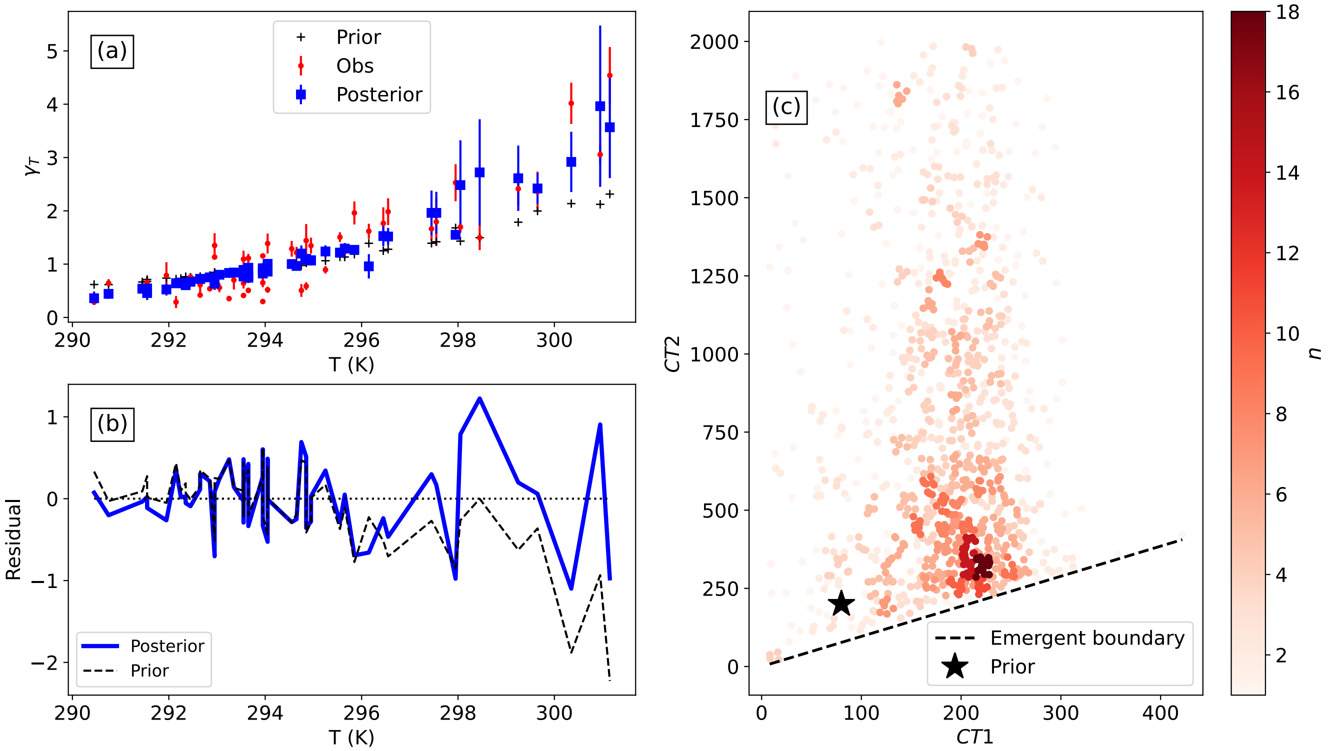

Figure 7. Metropolis-Hastings Markov Chain Monte Carlo optimization results for C_{T1} and C_{T2} parameters at WYT field site. (a) The observations, prior γ_T model, and posterior γ_T model. (b) The prior and posterior residuals. (c) The 2D posterior probability distribution of C_{T1} and C_{T2}, with darker colors indicating higher probability. The a priori parameterization is indicated by the black star, and the dashed black line indicates an emergent boundary.

The ability of the MHMCMC method to optimize model parameters is strongly limited by the observation error which appears in the denominator of Equation 8. Figure S5 in Supporting Information S1 shows MHMCMC parameter optimizations for three additional measurement sites (AABC, ALH, and ACM) with their observation errors artificially deflated to a small constant value of 0.05. While none of these configurations could be constrained by the MHMCMC when the actual observation errors were used, all of them could be constrained when using the artificially deflated errors.

4. Discussion

4.1. Variability of γ_T Across Ecosystems

There is large variability in the measured isoprene emission temperature response among the different field sites, as indicated by the large range of observed Q_{10}. This variability could be due to physiological differences between vegetation species. In particular, it may reflect differing stress tolerances of the local vegetation at each field site. The production of isoprene in plant leaves is believed to contribute to abiotic stress tolerance, possibly protecting vegetation from heat stress, drought, herbivory, and oxidation from radicals like ozone (Monson et al., 2021). Based on genetic evidence, it is believed that isoprene emission capacity has evolved independently many times throughout the plant kingdom (Harley et al., 1999; Sharkey et al., 2005). The mechanism by which isoprene protects plants from stress is unknown; previous studies suggested that isoprene helps stabilize cell membranes and quench oxidants through direct reaction (Sharkey et al., 2008), but subsequent work found that isoprene concentrations within plant tissues are not high enough for this to be plausible (Harvey et al., 2015). A more current hypothesis is that isoprene production is associated with beneficial protein production within plant leaves (Monson et al., 2021). In any case, the observed variability in γ_T may reflect differing physiological stress responses from vegetation to the local environment, which may be plausible given the wide range of ecosystems studied here.

Alternatively, the observed variability could be due differences in the canopy structure of different ecosystems. The PCEEA implementation of γ_T is parameterized based on a full canopy physics simulation for warm broadleaf forests; it would therefore be unsurprising to see differences in model performance for other canopy environments, and indeed this implementation has been shown to produce local biases relative to full canopy physics models despite good global agreement (Guenther et al., 2006). Discerning between physiological and canopy-related effects requires leaf temperature measurements, which were not available at most field sites. We discuss this source of error in Section 4.3.2.

Of the four boreal-Arctic sites, three showed higher temperature sensitivity than the a priori γ_T parameterization: ACM, ABK, and SNA. This is consistent with previous studies of high-latitude vegetation. For example, using enclosure measurements of tundra vegetation at a Northern Alaska field site, Angot et al. (2020) found that isoprene emissions continued to increase at air temperatures above 30°C, whereas MEGAN predicted a decline in emissions at these temperatures. Another study using enclosure measurements over the course of a growing season found that the measured isoprene temperature response was roughly 50% steeper than MEGAN predictions for subarctic *Salix mysinites* and *Betula nana* shrubs (Li et al., 2023). Kramshøj et al. (2016), Seco et al. (2020, 2022), and Vettikkat et al. (2023) similarly found increased temperature sensitivity for isoprene emissions from high-latitude vegetation. At the ABK site, similar results were obtained regardless of whether air temperature or leaf temperature was used to calculate γ_T, suggesting that the observed high temperature sensitivity is a physiological property of the vegetation and not related to the parameterization of the air-temperature/leaf temperature relationship in the canopy. Conversely, nearby wetland measurements reported by Seco et al. (2020) showed large differences between air-temperature and leaf-temperature derived temperature sensitivity (see Section 4.3.2).

In contrast to these sites, the observations at the Norwegian FNS site were in good agreement with the a priori γ_T parameterization. This is true with both air and leaf temperature measurements, again suggesting a physiological explanation. There are fairly large differences in vegetation at FNS compared to the other two Fennoscandian sites ABK and SNA, possibly because FNS is an alpine site at higher elevation above sea level (1,222 m) compared to ABK (360 m) or SNA (162 m). Similarly, the ACM site is at a relatively low elevation of 270 m above sea level. Despite its distance from the other sites, the vegetation at ACM is similar to ABK and SNA, including abundant *Sphagnum* mosses and *Eriophorum vaginatum* sedges. Recent work by H. Wang et al. (2024b) has demonsrated that sedges in particular are responsible for the high isoprene emission rates measured at several high-latitude sites.

The observations were in good agreement with the a priori γ_T parameterization at AABC and CTV in central Alabama and CTP in Italy. However, the measured temperature sensitivity at the ALH and WYT sites in the United Kingdom was significantly higher than the a priori γ_T. Isoprene emissions at all five of these sites are dominated by *Quercus* (oak trees), but the species and climatic conditions are not the same: *Quercus robur* (European oak) dominates at ALH and WYT, *Quercus ilex* (holm oak) and *Quercus suber* (cork oak) dominate at CTP, and none of these species are present at the North American AABC and CTV sites. In terms of climate, the ALH and WYT sites experience generally cooler growing seasons compared to the Italian and North American sites, which likely impacts the heat stress response of local vegetation. These results suggest that *Quercus robur* is more sensitive to temperature than the oak species found at the lower-latitude sites, or alternatively, the individual specimens at ALH and WYT may be more sensitive to temperature due to their generally cooler growing conditions during spring and summer. Another study of a Mediterranean oak forest *(Quercus pubsecens*) in southern France found good agreement with the modeled temperature and sunlight response $\gamma_T \times \gamma_{PAR}$ (Kalogridis et al., 2014); while they did not specifically investigate the parameterization of γ_T, this is further evidence that the vegetation at the UK sites ALH and WYT responds differently to temperature variations than oaks from warmer regions. A previous study of North American oak species in the Missouri Ozarks found significant differences in both temperature and drought sensitivity for different species (Geron et al., 2016), so it is unsurprising that we see different behavior amongst our oak-dominated sites in this study.

The observed temperature sensitivity at the ATTO site in the Amazon rainforest is in good agreement with the a priori γ_T parameterization. This is in stark contrast with the observations at the STM site (Figure S1 in Supporting Information S1), also in the Amazon rainforest ~460 km east of ATTO. The measurements at both sites were taken from towers above a closed broadleaf forest canopy. The dominant vegetation species at each site are different, with STM being primarily *Erisma uncinatum Warm., Carapa guianensis Aubl., Manilkara huberi*

(Ducke) A. Chev., and *Protium sp.* (Gonçalves and Santos, 2008) and ATTO featuring *Pouteria*, *Pourouma*, *Helicostylis*, and *Cecropia* (Mota de Oliveira et al., 2022). It is possible that the STM vegetation, which is adapted to the comparatively drier conditions of the Eastern Amazon basin (Nepstad et al., 1994; Saleska et al., 2003), exhibits higher temperature sensitivity than vegetation found in the more humid central and Western portions of the basin.

Previous studies have already demonstrated variability in γ_T in tropical ecosystems, and our results are consistent with this. In particular, multiple field and laboratory studies have found increased temperature sensitivity for tropical vegetation. Langford et al. (2010) found a two-fold increase in E_{Opt} (the maximum value of γ_T described by Equation 4) in a tropical rainforest in Malaysia's Sabah region, consistent with laboratory experiments for tropical *Ficus* trees (Oku et al., 2008). Similarly, Misztal et al. (2011) found higher T_{MAX} for oil palms in Malaysian Borneo, in agreement with laboratory measurements of Wilkinson et al. (2006). In Australia, Emmerson et al. (2020) found up to three-fold increases in E_{Opt} using laboratory measurements of *Eucalypt* species. Given this large variability, there is some precedent for the differences we observed between the ATTO and STM sites.

4.2. Strong Thermal Hysteresis Effect at Several Mid-To-High Latitude Field Sites

The heightened temperature sensitivity of isoprene emissions at several field sites (ABK, SNA, WYT) was successfully modeled by γ_T when the value of the K_2 parameter was increased in the MHMCMC optimization (Figure 6), leading to improved model-observation agreement at high temperatures. An increase in K_2 produces a larger thermal hysteresis effect in Equation 4, which implies that the vegetation is responding more strongly to variations in average ambient temperatures (T_{24}) than predicted by the baseline γ_T parameterization. Vettikkat et al. (2023) previously found that isoprene emissions at SNA were elevated for several days after a period of anomalously hot weather, providing direct observational evidence for a strong thermal hysteresis effect which is captured in our optimized model. While the time scale of the observed thermal hysteresis effect at SNA is likely longer than 24 hr, we were still able to improve MEGAN's performance using only the K_2 parameter on 24-hr time scales. Other data sets not used in this study have also shown that the thermal hysteresis effect may be responsible for the heightened temperature sensitivity of high-latitude isoprene emissions compared to MEGAN predictions, especially for sedge species (H. Wang et al., 2024a, 2024b). Our optimization results are consistent with these findings.

Underestimating the temperature sensitivity of emissions has been shown in other studies to lead to underpredictions of isoprene emissions during high-temperature periods (Emmerson et al., 2020; Vettikkat et al., 2023). This may be especially problematic for emission modeling at high latitudes because the arctic region is warming significantly faster than the rest of the planet (England et al., 2021). Our results suggest that a simple re-parameterization of the thermal hysteresis effect in γ_T can account for much of the observed temperature sensitivity, which will allow for more accurate modeling of arctic isoprene emissions and their impacts on atmospheric chemistry as the region warms. In other regions, we expect the increased temperature sensitivity of emissions to be important during heatwaves. For example, while DiMaria et al. (2023) found good agreement between γ_T and isoprene observations at WYT using a short time series in May 2018, here we find significant disagreements at high temperatures which were easily accounted for by increasing the strength of thermal hysteresis via the K_2 parameter. Even if anomalously high temperatures are infrequent (as is the case with the filtered WYT time series data), the exponential relationship between emissions and temperature means that such events have a disproportionately large impact on isoprene emissions. Furthermore, the increasing frequency of heatwaves (Perkins-Kirkpatrick et al., 2012; Perkins-Kirkpatrick & Lewis, 2020) in many regions of the world indicates that accurately modeling the temperature sensitivity of isoprene emissions will be increasingly important in the future.

Overall, our results illustrate the importance of accurately parameterizing the thermal hysteresis effect in γ_T for a variety of vegetation types. We have shown that isoprene flux and concentration measurements can be used for this purpose. Controlled experiments should also be performed to measure γ_T under a range of ambient temperature conditions. This would make it possible to conclusively determine whether the thermal hysteresis effect is responsible for the increased temperature sensitivity observed at our field sites. The recent measurements of H. Wang et al. (2024b) strongly suggest that the increased strength of the thermal hysteresis effect at arctic field sites is a real physiological effect.

4.3. Uncertainties and Limitations

The analysis presented in this study is subject to several important limitations and sources of uncertainty. In addition to observation errors and the low sensitivity of γ_T to its parameterization, there are four other major sources of uncertainty which affect the interpretation of our optimization experiments. These are the lack of leaf temperature measurements at most field sites, the impact of non-temperature sources of isoprene variability, the reliance on concentration rather than flux measurements at some field sites, and equifinality which makes interpretation of the optimized parameters difficult. These are discussed in the following subsections. We also discuss how uncertainties in γ_T fit into the broader context of isoprene emission modeling, which is subject to many other sources of error such as landcover and drought stress uncertainties.

4.3.1. Observation-Related Limitations: Low Parameter Sensitivity and Time Series Length

The most significant obstacle to our γ_T optimization experiments is the relatively low sensitivity of γ_T to its parameterization at ordinary ambient temperatures. In most cases the optimized posterior γ_T parameterization is indistinguishable from the a priori parameterization at low temperatures. The severity of this problem depends on the precision of the observations, as more precise observations allow us to observe smaller changes in γ_T due to changing parameters. Constraining the model parameters therefore requires sufficiently precise observations at higher temperatures where the parameters have a larger impact. Since anomalously high temperatures are by-definition uncommon, longer time series measurements are helpful for ensuring we properly sample this regime. The WYT data set provides the best example of the importance of high-temperature observations. DiMaria et al. (2023) found no significant discrepancies between the observations and the a priori γ_T parameterization at this site when using a shorter subset of the data that did not include enough high temperature observations. In this study, we found similarly good agreement between the observations and the a priori γ_T at low temperatures, but significant discrepancies at higher temperatures. This is clear justification for measuring longer time series, ideally spanning seasonal or interannual timescales, in order to avoid sampling biases. The use of longer time series does require more careful data filtering to deal with seasonal variability related to changes in LAI, leaf age, and soil moisture (see Section 4.3.3), so concurrent measurements of these quantities would also be required.

Since it may not always be feasible to collect long time series records, especially in remote regions of the tropics or the Arctic, another solution is to perform direct measurements of isoprene fluxes from vegetation over a wide range of temperatures to constrain γ_T as was done in Emmerson et al. (2020) for Australian *Eucalypt* trees. That study used a laboratory environment where the environmental conditions including air temperature could be precisely controlled. This approach ensures that the data used to train the optimized γ_T parameterization cover a sufficiently wide range of temperatures with minimal confounding effects from other environmental variables, something that is not always possible with time series measurements.

4.3.2. Leaf Temperature and Simplified Canopy Parameterizations

Isoprene emission rates depend on leaf temperature, which can be substantially different than ambient air temperature in some ecosystems. The lack of leaf surface temperature measurements at most of the field sites makes it impossible to determine whether the observed errors in γ_T are due to physiological properties of the local vegetation, or whether they instead reflect errors in the relationship between air temperature and leaf temperature; this relationship is implicit in the parameterization of γ_T when using air temperature as a model input and depends on radiative transfer within the vegetation canopy. The PCEEA implementation has been shown to lead to local biases relative to full canopy models (Guenther et al., 2006), including at the ALH and CTP field sites used in this study (Fares et al., 2013; Langford et al., 2017). We do not have leaf temperature measurements at SNA, but a full 5-layer canopy physics simulation showed that air leaf temperature was typically within 1°C of the ambient air temperature at that site (Vettikkat et al., 2023). At ABK and FNS, we found no significant differences in temperature sensitivity (as quantified by Q_{10}) when using measured air temperature or leaf temperature. On the other hand, Seco et al. (2020) found that the measured temperature sensitivity at a wetland site near our ABK site was nearly 10× greater when using leaf temperature rather than air temperature measurements to calculate γ_T. It is therefore clear that even though leaf temperature measurements did not have a significant impact on the measured temperature sensitivity in our study, we cannot assume this will be true for other sites. This uncertainty extends beyond isoprene emission modeling. A recent study has found that for high-latitude vegetation in particular, differences between air and leaf temperature can lead to large errors in hydrological and carbon cycle models (Tang et al., 2024). Leaf temperature measurements should be made whenever possible to reduce these sources of error.

This issue can be partially addressed by using an explicit canopy model to calculate γ_T instead of the simplified PCEEA implementation as was done by Vettikkat et al. (2023) at SNA, but doing this globally requires accurate representations of a broad range of canopy environments and additional driving variables to simulate radiation and atmospheric transport processes. Attempts to reduce this complexity in global models using machine learning approaches have been shown to introduce ecosystem-dependent emission biases, but they do show reasonably good agreement with full canopy physics models (Silva et al., 2020). Other studies like Emmerson et al. (2020) have avoided the canopy model issue entirely by measuring γ_T directly at the leaf-level in laboratory experiments, which allows for the unambiguous observation of physiological effects. Similarly, repeating our optimization experiments with a full canopy physics model like MEGAN3 would help to disentangle the effects of canopy environment and plant physiology and would therefore be worthwhile. However, using parameters derived from full canopy physics simulations or leaf-level measurements in global atmospheric models will inevitably require the use of a simplified canopy parameterization. Despite the uncertainties associated with the simplified PCEEA parameterization, its ease of use in global models made it a sensible choice for this study.

4.3.3. Data Filtering Uncertainties

Non-temperature related isoprene variability can be mistakenly attributed to γ_T if it is not properly accounted for via data filtering. While we are confident in the data filtering methodology described in Section 2.3.1, there are a few caveats worth addressing. First, our data sets do not include leaf age measurements, even though leaf age is known to impact isoprene emission capacity (Alves et al., 2016, 2018; Guenther et al., 2006). Many of our data sets contain LAI measurements, and while there are algorithms for calculating the leaf age activity factor γ_{AGE} based on changes in total LAI, this approach is less effective in situations where leaf total area is relatively constant such as in tropical broadleaf forests. Because leaf age primarily impacts emissions during seasonal transitions when there are large populations of young or senescing leaves (Alves et al., 2018), this can be partially avoided by using relatively short time series and avoiding the beginning and end of the growing season. However, as discussed in Section 4.3.1, the use of short time series introduces a different source of error where we may not be adequately sampling high-temperature periods, as was the case at the WYT site in DiMaria et al. (2023). It would therefore be preferable to obtain longer time series with sufficient ancillary measurements to account for emission variability due to LAI, leaf age, and soil moisture.

Our analysis at the SNA site may be impacted by leaf age, as it spans the beginning of the local growing season during a time of rapid foliage expansion; this may lead to an overestimate of the measured temperature sensitivity at SNA, as increasing temperatures are correlated with leaf maturation. The other important caveat is drought stress. While we are confident that this was not an issue at our field sites based on the arguments presented in Section 2.3.1, we cannot definitively rule it out without measurements of soil moisture and knowledge of the vegetation wilting point at the measurement sites. The importance of drought stress in isoprene emission modeling is being increasingly recognized (Potosnak et al., 2014; Seco et al., 2015; Jiang et al., 2018; Bamberger et al., 2017; Otu-Larbi et al., 2020; Y. Wang et al., 2022; H. Wang et al., 2022), and future measurement campaigns should ensure necessary observations are obtained to quantify this effect.

4.3.4. Uncertainties Associated With Mixing Ratio Measurements

As discussed previously, deriving γ_T from mixing ratio measurements requires that we account for variability in atmospheric dispersion and photochemical losses. Photochemical loss rate variability is strongly coupled to sunlight-driven OH production, so this is largely accounted for by filtering for high-PPFD observations. At three of our field sites (AABC, CTV, and WYT), dispersion is the dominant loss process, so this is likely not a large source of error. However, this argument may not be valid at the ATTO field site due to the longer lifetime of isoprene in the Amazon (Palmer et al., 2022), as well as the fact that the ATTO site is surrounded in all directions by isoprene emission sources for very large distances. An additional complicating factor is that isoprene suppresses its own OH sink when emissions are high enough, leading to a non-linear relationship between isoprene emissions and atmospheric concentrations (Feiner et al., 2016; Fu et al., 2019). However, GEOS-Chem (The International GEOS-Chem User Community, 2021) model results suggest that this non-linearity can be mostly

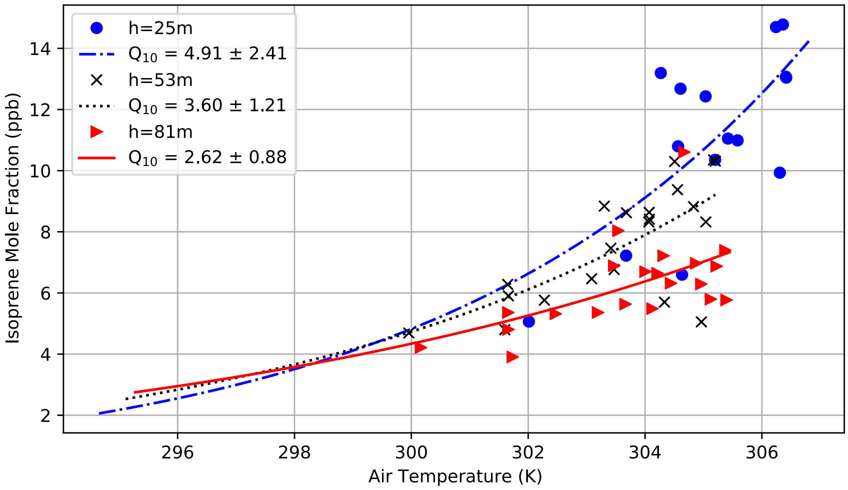

Figure 8. Observed temperature response at ATTO $h = 81$ m (red triangles), $h = 53$ m (black crosses), and $h = 25$ m (blue circles). An exponential fit using Equation 6 is shown for each measurement height: 25 m (dashed-dotted blue), 53 m (dotted black), and 81 m (solid red). Note that he 25 m elevation measurements are below the mean forest canopy height of 35 m.

eliminated by filtering the observations for sunlight and WS/direction (i.e., photochemical and dispersive loss rates) in midlatitude regions (see Figure S6 in Supporting Information S1), and to a lesser extent in tropical regions like the Amazon Basin (see Figure S7 in Supporting Information S1). Additional non-linearity might be introduced by temperature-dependent NO_x emissions from soils (Hudman et al., 2012). A reduction in the atmospheric isoprene lifetime driven by increased NO_x emissions at high temperatures could effectively dampen the derived temperature sensitivity of isoprene emissions, because higher isoprene emission rates would be correlated with reduced isoprene lifetimes and a consequently smaller buildup of atmospheric isoprene concentrations. Concurrent NO_x measurements would be required to quantify this effect.

A final issue with mixing ratio measurements is that the temperature dependence of atmospheric isoprene concentrations depends on the altitude at which measurements are made, with higher altitude measurements showing less sensitivity to temperature than lower altitude measurements (Kalogridis et al., 2014). This can be clearly seen at the ATTO field. The ATTO measurements presented earlier were taken at a height of 81 m above ground level, which is well-above the mean local canopy height of 35 m. In Figure 8 we have repeated the filtering process described in Section 2.3.1 for two additional elevations (25 and 53 m above ground level). There are large differences in the measured temperature response at these three altitudes. However, the measurements at $h = 25$ m are within the forest canopy and thus are not suitable as proxies for canopy scale isoprene fluxes, and the differences between the $h = 53$ m and $h = 81$ m measurements are too small to be distinguishable by our MHMCMC optimization given the large amount of scatter and relatively large measurement uncertainties. In any case, while isoprene mixing ratio measurements are extremely valuable, we recognize that interpreting them in terms of isoprene emission rates is more uncertain than using eddy covariance flux measurements.

4.3.5. Equifinality

The final major obstacle for interpretation is equifinality, wherein different combinations of parameters and model inputs yield the same output. Uncertainties in model inputs were previously found to be a large source of error in isoprene emission model optimization (DiMaria et al., 2023), which we effectively avoid here by exclusively relying on locally measured meteorological variables and avoiding the use of other model components in our calculations (except at the SNA site where we used γ_{LAI}). Despite these improvements, there is always the possibility of inappropriately using model parameters as "tuning knobs" to improve model-observation agreement without sufficient physical justification. An example of this problem is the MHMCMC optimization at the WYT field site; in Figure 6(c) we improve the model performance by optimizing K_2, but in Figure 7 we achieve similar improvements optimizing C_{T1} and C_{T2}. The emergent boundary in Figure 7 also shows that posterior parameters can be correlated with each other (in this case C_{T1} and C_{T2}). It is for this reason that we focused primarily on the optimization of the K_2 parameter, since it is easy to interpret the impact of this parameter on emissions in physical terms (i.e., it controls the strength of the thermal hysteresis effect). The recent studies of H. Wang et al. (2024a, 2024b), H. Wang, Nagalingam, et al. (2024) suggest that focusing on the thermal hysteresis effect is appropriate for sedges which are present at the high-latitude sites used in this study. Overall, we adopt the view that parameter optimizations which use a smaller number of easily interpretable free parameters are better than those which rely on more parameters, or those which cannot be easily explained in terms of physical processes.

4.3.6. Temperature Response Uncertainties in the Context of Isoprene Emission Modeling

Optimizing the temperature response of modeled isoprene emissions can reduce model biases and produce more realistic temporal variability of modeled emissions, but these improvements must be considered in the context of other uncertainties in isoprene emission modeling. Basal emission factors, which quantify the emission capacity of vegetation at various spatial scales, are thought to be the largest source of error in isoprene emission models (Guenther et al., 2012; Langford et al., 2010). Calculation of these emission factors for use in global models requires representative isoprene emission measurements for each vegetation or ecosystem type. In practice, emission factors in global models are typically extrapolated based on measurements for a particular plant functional type due to a lack of observation coverage, particularly in remote regions and the tropics (Guenther et al., 2006, 2012; Marais et al., 2014). This is a source of error due to uncertainties in vegetation distributions as well as the large variability in isoprene emission capacities among plant species, including those that are closely related (Batista et al., 2019; Guenther et al., 1993; Li et al., 2021). An additional source of error is that the calculation of basal emission factors relies on activity factors including γ_T to normalize measured isoprene fluxes to pre-defined "standard" meteorological conditions (Kalgoridis et al., 2014; Langford et al., 2017; Niinemets et al., 2011). Uncertainties in land use and landcover, including plant functional type distributions, also impact isoprene emission models (Arneth et al., 2011; Guenther et al., 2006; Opacka et al., 2021; Pfister et al., 2008).

Like the temperature response γ_T, the emission sensitivity to sunlight (γ_{PAR}), leaf area (γ_{LAI}), leaf age (γ_{AGE}), and soil moisture (γ_{SM}) are empirically parameterized based on observations and are subject to uncertainties. Emission sensitivity to sunlight is generally less pronounced than the temperature sensitivity because γ_T exhibits exponential growth up to relatively high temperatures (Guenther et al., 2006); nevertheless, γ_{PAR} is uncertain and observations from a variety of vegetation types have shown significant deviations from the a priori γ_{PAR} parameterization (e.g., Langford et al., 2017, 2022). Sensitivity of emissions to LAI and leaf age can be significant on monthly to seasonal timescales, particularly in low-LAI environments where γ_{LAI} is not saturated due to the square-root dependance of γ_{LAI} on LAI (Guenther et al., 2006) and during seasonal transitions with large populations of young or senescing leaves (Alves et al., 2018). The soil moisture activity factor γ_{SM} has received significant attention in recent years and is increasingly being recognized as a major driver of isoprene emission variability during periods of drought stress (Bamberger et al., 2017; Jiang et al., 2018; Opacka et al., 2022; Otu-Larbi et al., 2020; Potosnak et al., 2014; Seco et al., 2015; Y. Wang et al., 2022; H. Wang et al., 2022). Moderate drought stress can lead to an increase in emissions and changes in the emission temperature sensitivity (Potosnak et al., 2014; H. Wang et al., 2022: see also Figure 3j), while severe drought stress leads to a reduction in emissions.

There have been improvements to MEGAN with the release of version 3 (Guenther et al., 2020). Many have focused on the calculation of the basal emission factors (Guenther et al., 2020) as well as the representation of the drought stress response γ_{SM} (Jiang et al., 2018; Otu-Larbi et al., 2020; Y. Wang et al., 2022; H. Wang et al., 2022). Further reducing uncertainties in γ_T would add to these efforts and lead to more accurate isoprene emission models, such as the recent work by H. Wang et al. (2024a, 2024b), H. Wang, Nagalingam, et al. (2024) for Arctic and urban vegetation.

5. Conclusions

We showed that the temperature sensitivity of isoprene emissions was highly variable across a range of field sites in different ecosystems. In particular, the temperature sensitivity at many sites was higher than predicted by the existing γ_T model. We found that γ_T could be reparametrized using MHMCMC data assimilation at several field sites, leading to improved model-observation agreement. Increasing the strength of the thermal hysteresis effect yielded the most promising results, allowing γ_T to model the rapid increase in emissions at high temperatures while not altering its behavior at lower temperatures. This allowed us to accurately model the observed temperature sensitivity at two high-latitude field sites and a UK field site where the original γ_T parameterization was inadequate.

Future work should continue to prioritize the collection of isoprene flux measurements in a diverse range of ecosystems to quantify the variability of γ_T. We especially encourage measurements in underrepresented regions such as the Arctic and the tropics. Measurements in urban areas will also be useful to accurately model the air quality impacts of urban greening efforts in a warming climate (Wei et al., 2024). Due to the low sensitivity of γ_T to its parameterization at typical ambient temperatures, controlled experiments with leaf-level flux measurements should be used to directly measure the thermal hysteresis effect where possible. This method would eliminate the ambiguity in our interpretation of the optimized parameterization (i.e., physiological differences vs. air-temperature/leaf-temperature relationships) and would also reduce uncertainties related to the use of small data sets in the γ_T optimization. Specifically, the differences in the observed temperature response at Wytham Woods in this study compared to DiMaria et al. (2023) showed that the optimization is critically dependent on having enough high-temperature observations to see the effects of errors in the γ_T parameterization. In cases where such experiments are not feasible, we can still gain valuable information about the γ_T parameterization from canopy-scale flux or mixing ratio measurements provided that ancillary meteorological data are available for observation filtering, and that the measurements are sufficiently precise to be able to discriminate between different γ_T parameterizations. In these cases, collecting longer time series on seasonal-to-interannual scales will help reduce sampling biases, which will be especially useful for constraining emission responses during stressful but relatively uncommon periods such as severe heatwaves and droughts.

Given the large variability in the isoprene emission temperature response across ecosystems and vegetation species, the long-term goal of this work is to develop an ecosystem-specific parameterization of γ_T that can be used in global isoprene emission models. The parameterization of γ_T could then be tied to specific landcover or plant functional types in the same way as basal emission factors. Using global chemical transport models, the impact of the updated γ_T parameterization on air quality and climate pollutants could be quantified. This will inevitably require a very large observational data set with which we can constrain γ_T. To that end, we strongly encourage the publication of existing isoprene measurements, along with ancillary meteorological and environmental observations, in publicly accessible repositories. The coordinated publication of these data in a centralized location would greatly facilitate model optimization and development work and would allow researchers to readily extend the analysis presented here to a wider variety of ecosystems.

Acknowledgments

C.A. DiMaria acknowledges a Canada Graduate Scholarship—Doctoral (CGS D) Grant funded by the Natural Sciences and Engineering Research Council of Canada (NSERC) (application no. PGSD3-546,721–2020). This work was also supported by Grant 16SUASEMIS from the Canadian Space Agency. Part of this work was carried out at the Jet Propulsion Laboratory, California Institute of Technology, under a contract with the National Aeronautics and Space Administration (NASA). We acknowledge the support and guidance from the staff at the University of Oxford's Wytham Woods, and the UK Natural Environment Research Council (NE/W003694/1) for financial support. The Danish National Research Foundation supported activities within the Center for Volatile Interactions (VOLT, DNRF168). We thank the Instituto Nacional de Pasquisas da Amazonia (INPA) and the Max Planck Society for continuous support. AMYS acknowledges the support by the ATTO project (German Federal Ministry of Education and Research, BMBF funds 01LB1001A; Brazilian Ministério da Ciência, Tecnologia e Inovação FINEP/MCTI contract 01.11.01248.00); UEA and FAPEAM, LBA/INPA and SDS/CEUC/RDS-Uatumã. We acknowledge the Swedish Polar Research Secretariat and SITES for the support of the work done at the Abisko Scientific Research Station. SITES is supported by the Swedish Research Council's Grant 4.3-2021-00164. Part of this work was supported by the Research Council of Finland (Grants 310682, 337550, 346371, 357905). R. S. acknowledges a Ramón y Cajal Grant (RYC2020-029216-I) funded by MICIU/AEI/10.13039/501100011033 and by "ESF Investing in your future," and project PID2021-122892NA-I00 funded by MICIU/AEI and by "ERDF A way of making Europe."

Data Availability Statement

A repository containing all data and code necessary to reproduce our analysis is available at https://doi.org/10.5281/zenodo.15262183 (DiMaria et al., 2025). The MEGAN 2.1 source code can be obtained from https://bai.ess.uci.edu/megan/data-and-code (Guenther, 2024). The original MHMCMC Matlab code upon which our work is based is available at https://doi.org/10.5281/zenodo.4904195 (Yang et al., 2021). All isoprene measurements and ancillary meteorological measurements used in this study are publicly available and can be obtained from the references listed in Table 1. Historical weather records were obtained from Visual Crossing (https://www.visualcrossing.com/weather-history; Last Accessed: 29 October 2023) to screen for drought conditions in cases where soil moisture measurements were not available.

References

Alves, E. G., Jardine, K., Tota, J., Jardine, A., Yãnez-Serrano, A. M., Karl, T., et al. (2016). Seasonality of isoprenoid emissions from a primary rainforest in central Amazonia. *Atmospheric Chemistry and Physics*, *16*(6), 3903–3925. https://doi.org/10.5194/acp-16-3903-2016

Alves, E. G., Tóta, J., Turnipseed, A., Guenther, A. B., Vega Bustillos, J. O., Santana, R. A., et al. (2018). Leaf phenology as one important driver of seasonal changes in isoprene emissions in Central Amazonia. *Biogeosciences*, *15*(13), 4019–4032. https://doi.org/10.5194/bg-15-4019-2018

Angot, H., McErlean, K., Hu, L., Millet, D. B., Hueber, J., Cui, K., et al. (2020). Biogenic volatile organic compound ambient mixing ratios and emission rates in the Alaskan Arctic tundra. *Biogeosciences*, *17*(23), 6219–6236. https://doi.org/10.5194/bg-17-6219-2020

Arneth, A., Schurgers, G., Lathiere, J., Duhl, T., Beerling, D. J., Hewitt, C. N., et al. (2011). Global terrestrial isoprene emission models: Sensitivity to variability in climate and vegetation. *Atmospheric Chemistry and Physics*, *11*(15), 8037–8052. https://doi.org/10.5194/acp-11-8037-2011

Bamberger, I., Ruehr, N. K., Schmitt, M., Gast, A., Wohlfahrt, G., & Arneth, A. (2017). Isoprene emission and photosynthesis during heatwaves and drought in Black Locust. *Biogeosciences*, *14*(15), 3649–3667. https://doi.org/10.5194/bg-14-3649-2017

Batista, C. E., Ye, J., Ribeiro, I. O., Guimarães, P. C., Medeiros, A. S., Barbosa, R. G., et al. (2019). Intermediate-scale horizontal isoprene concentrations in the near-canopy forest atmosphere and implications for emission heterogeneity. *Proceedings of the National Academy of Sciences*, *116*(39), 19318–19323. https://doi.org/10.1073/pnas.1904154116

Bloom, A. A., Bowman, K. W., Liu, J., Konings, A. G., Worden, J. R., Parazoo, N. C., et al. (2020). Lagged effects regulate the inter-annual variability of the Tropical Carbon Balance. *Biogeosciences*, *17*(24), 6393–6422. https://doi.org/10.5194/bg-17-6393-2020

Bloom, A. A., Worden, J., Jiang, Z., Worden, H., Kurosu, T., Frankenberg, C., & Schimel, D. (2015). Remote-sensing constraints on South America fire traits by Bayesian fusion of atmospheric and surface data. *Geophysical Research Letters*, *42*(4), 1268–1274. https://doi.org/10.1002/2014gl062584

Bourtsoukidis, E., Pozzer, A., Williams, J., Makowski, D., Peñuelas, J., Matthaios, V. N., et al. (2024). High temperature sensitivity of monoterpene emissions from global vegetation. *Communications Earth & Environment*, *5*(1), 23. https://doi.org/10.1038/s43247-023-01175-9

Brown, L. A., Ogutu, B. O., & Dash, J. (2020). Tracking forest biophysical properties with automated digital repeat photography: A fisheye perspective using digital hemispherical photography from below the canopy. *Agricultural and Forest Meteorology*, *287*, 107944. https://doi.org/10.1016/j.agrformet.2020.107944

Chen, W. H., Guenther, A. B., Wang, X. M., Chen, Y. H., Gu, D. S., Chang, M., et al. (2018). Regional to global biogenic isoprene emission responses to changes in vegetation from 2000 to 2015. *Journal of Geophysical Research: Atmospheres*, *123*(7), 3757–3771. https://doi.org/10.1002/2017jd027934

Claeys, M., Graham, B., Vas, G., Wang, W., Vermeylen, R., Pashynska, V., et al. (2004). Formation of secondary organic aerosols through photooxidation of isoprene. *Science*, *303*(5661), 1173–1176. https://doi.org/10.1126/science.1092805

Dias-Junior, C., Araujo, A., Soergel, M., Manzi, A. O., de Oliveira, M., & Teixeria, P. (2014). Micrometeorologic dataset - weather station (AWS) 2014 [Dataset]. *ATTP Data Portal*. https://www.attodata.org/ddm/data/Showdata/105

DiMaria, C. A., Jones, D. B., Worden, H., Bloom, A. A., Bowman, K., Stavrakou, T., et al. (2023). Optimizing the isoprene emission model Megan with satellite and ground-based observational constraints. *Journal of Geophysical Research: Atmospheres*, *128*(4), e2022JD037822. https://doi.org/10.1029/2022jd037822

DiMaria, C. A., Jones, D. B. A., Ferracci, V., Bloom, A. A., Worden, H. M., Seco, R., et al. (2025). Optimizing the Temperature Sensitivity of the Isoprene Emission Model MEGAN in Different Ecosystems Using a Metropolis-Hastings Markov Chain Monte Carlo Method [Software]. *Zenodo*. https://doi.org/10.5281/ZENODO.15262184

Emmerson, K. M., Possell, M., Aspinwall, M. J., Pfautsch, S., & Tjoelker, M. G. (2020). Temperature response measurements from eucalypts give insight into the impact of Australian isoprene emissions on air quality in 2050. *Atmospheric Chemistry and Physics*, *20*(10), 6193–6206. https://doi.org/10.5194/acp-20-6193-2020

England, M. R., Eisenman, I., Lutsko, N. J., & Wagner, T. J. (2021). The recent emergence of Arctic amplification. *Geophysical Research Letters*, *48*(15), e2021GL094086. https://doi.org/10.1029/2021gl094086

Fall, R., & Wildermuth, M. C. (1998). Isoprene synthase: From biochemical mechanism to emission algorithm. *Journal of Geophysical Research*, *103*(D19), 25599–25609. https://doi.org/10.1029/98jd00808

Fares, S., Schnitzhofer, R., Jiang, X., Guenther, A., Hansel, A., & Loreto, F. (2013). Observations of diurnal to weekly variations of monoterpene-dominated fluxes of volatile organic compounds from Mediterranean forests: Implications for regional modeling. *Environmental Science & Technology*, *47*(19), 11073–11082. https://doi.org/10.1021/es4022156

Feiner, P. A., Brune, W. H., Miller, D. O., Zhang, L., Cohen, R. C., Romer, P. S., et al. (2016). Testing atmospheric oxidation in an Alabama Forest. *Journal of the Atmospheric Sciences*, *73*(12), 4699–4710. https://doi.org/10.1175/jas-d-16-0044.1

Ferracci, V., Bolas, C. G., Freshwater, R. A., Staniaszek, Z., King, T., Jaars, K., et al. (2020). Continuous isoprene measurements in a UK temperate forest for a whole growing season: Effects of drought stress during the 2018 heatwave. *Geophysical Research Letters*, *47*(15), e2020GL088885. https://doi.org/10.1029/2020gl088885

Ferracci, V., Harris, N., Bolas, C., Jones, R., & Staniaszek, Z. (2020). Biodiversity and land use impacts on tropical forest ecosystem function (BALI): Isoprene concentration measurements at Wytham Woods (UK) during the summer of 2018 [Dataset]. *Centre for Environmental Data Analysis*. https://catalogue.ceda.ac.uk/uuid/0c39809848ce47bb850d8ca2045e40f2

Fu, D., Millet, D. B., Wells, K. C., Payne, V. H., Yu, S., Guenther, A., & Eldering, A. (2019). Direct retrieval of isoprene from satellite-based infrared measurements. *Nature Communications*, *10*(1), 3811. https://doi.org/10.1038/s41467-019-11835-0

Geron, C., Daly, R., Harley, P., Rasmussen, R., Seco, R., Guenther, A., et al. (2016). Large drought-induced variations in oak leaf volatile organic compound emissions during Pinot Noir 2012. *Chemosphere*, *146*, 8–21. https://doi.org/10.1016/j.chemosphere.2015.11.086

Geron, C., Guenther, A. B., Sharkey, T., & Arnts, R. R. (2000). Temporal variability in basal isoprene emission factor. *Tree Physiology*, *20*(12), 799–805. https://doi.org/10.1093/treephys/20.12.799

Goldstein, A. H., Goulden, M. L., Munger, J. W., Wofsy, S. C., & Geron, C. D. (1998). Seasonal course of isoprene emissions from a midlatitude deciduous forest. *Journal of Geophysical Research*, *103*(D23), 31045–31056. https://doi.org/10.1029/98jd02708

Gonçalves, F. G., & Santos, J. R. (2008). Composição Florística e Estrutura de Uma Unidade de Manejo florestal sustentável na Floresta Nacional do Tapajós, Pará. *Acta Amazonica*, *38*(2), 229–244. https://doi.org/10.1590/s0044-59672008000200006

Guenther, A. (2024). MEGANv2.1 code, user guide, input files, global BVOC emissions output, test case [Software]. *Zenodo*. https://doi.org/10.5281/ZENODO.10525127

Guenther, A., Baugh, B., Brasseur, G., Greenberg, J., Harley, P., Klinger, L., et al. (1999). Isoprene emission estimates and uncertainties for the central African EXPRESSO study domain. *Journal of Geophysical Research: Atmospheres*, *104*(D23), 30625–30639. https://doi.org/10.1029/1999jd900391

Guenther, A. B., Hewitt, C. N., Erickson, D., Fall, R., Geron, C., Graedel, T., et al. (1995). A global model of natural volatile organic compound emissions. *Journal of Geophysical Research*, *100*(D5), 8873–8892. https://doi.org/10.1029/94jd02950

Guenther, A. B., Jiang, X., Heald, C. L., Sakulyanontvittaya, T., Duhl, T., Emmons, L. K., & Wang, X. (2012). The model of emissions of gases and aerosols from nature version 2.1 (MEGAN2.1): An extended and updated framework for modeling biogenic emissions. *Geoscientific Model Development*, *5*(6), 1471–1492. https://doi.org/10.5194/gmd-5-1471-2012

Guenther, A. B., Jiang, X., Shah, T., Huang, L., Kemball-Cook, S., & Yarwood, G. (2020). Model of emissions of gases and aerosol from nature version 3 (MEGAN3) for estimating biogenic emissions. *Springer Proceedings in Complexity*, 187–192. https://doi.org/10.1007/978-3-030-22055-6_29

Guenther, A. B., Karl, T., Harley, P., Wiedinmyer, C., Palmer, P. I., & Geron, C. (2006). Estimates of global terrestrial isoprene emissions using Megan (model of emissions of gases and aerosols from nature). *Atmospheric Chemistry and Physics*, *6*(11), 3181–3210. https://doi.org/10.5194/acp-6-3181-2006

Guenther, A. B., Zimmerman, P. R., Harley, P. C., Monson, R. K., & Fall, R. (1993). Isoprene and monoterpene emission rate variability: Model evaluations and sensitivity analyses. *Journal of Geophysical Research*, *98*(D7), 12609–12617. https://doi.org/10.1029/93jd00527

Haario, H., Saksman, E., & Tamminen, J. (2001). An adaptive Metropolis algorithm. *Bernoulli*, *7*(2), 223. https://doi.org/10.2307/3318737

Hanson, D. T., & Sharkey, T. D. (2001). Rate of acclimation of the capacity for isoprene emission in response to light and temperature. *Plant, Cell and Environment*, *24*(9), 937–946. https://doi.org/10.1046/j.1365-3040.2001.00745.x

Harley, P. C., Monson, R. K., & Lerdau, M. T. (1999). Ecological and evolutionary aspects of isoprene emission from plants. *Oecologia*, *118*(2), 109–123. https://doi.org/10.1007/s004420050709

Harvey, C. M., Li, Z., Tjellström, H., Blanchard, G. J., & Sharkey, T. D. (2015). Concentration of isoprene in artificial and thylakoid membranes. *Journal of Bioenergetics and Biomembranes*, *47*(5), 419–429. https://doi.org/10.1007/s10863-015-9625-9

Hidy, G. M., Blanchard, C. L., Baumann, K., Edgerton, E., Tanenbaum, S., Shaw, S., et al. (2014). Chemical climatology of the southeastern United States, 1999–2013. *Atmospheric Chemistry and Physics*, *14*(21), 11893–11914. https://doi.org/10.5194/acp-14-11893-2014

Holst, T., Arneth, A., Hayward, S., Ekberg, A., Mastepanov, M., Jackowicz-Korczynski, M., et al. (2010). BVOC ecosystem flux measurements at a high latitude wetland site. *Atmospheric Chemistry and Physics*, *10*(4), 1617–1634. https://doi.org/10.5194/acp-10-1617-2010

Hudman, R. C., Moore, N. E., Mebust, A. K., Martin, R. V., Russell, A. R., Valin, L. C., & Cohen, R. C. (2012). Steps towards a mechanistic model of global soil nitric oxide emissions: Implementation and space based-constraints. *Atmospheric Chemistry and Physics*, *12*(16), 7779–7795. https://doi.org/10.5194/acp-12-7779-2012

Jiang, X., Guenther, A., Potosnak, M., Geron, C., Seco, R., Karl, T., et al. (2018). Isoprene emission response to drought and the impact on global atmospheric chemistry. *Atmospheric Environment*, *183*, 69–83. https://doi.org/10.1016/j.atmosenv.2018.01.026

Kalogridis, C., Gros, V., Sarda-Esteve, R., Langford, B., Loubet, B., Bonsang, B., et al. (2014). Concentrations and fluxes of isoprene and oxygenated VOCs at a French Mediterranean oak forest. *Atmospheric Chemistry and Physics*, *14*(18), 10085–10102. https://doi.org/10.5194/acp-14-10085-2014

Kramshøj, M., Vedel-Petersen, I., Schollert, M., Rinnan, Å., Nymand, J., Ro-Poulsen, H., & Rinnan, R. (2016). Large increases in arctic biogenic volatile emissions are a direct effect of warming. *Nature Geoscience*, *9*(5), 349–352. https://doi.org/10.1038/ngeo2692

Langford, B., Cash, J., Acton, W. J., Valach, A. C., Hewitt, C. N., Fares, S., et al. (2017). Isoprene emission potentials from European oak forests derived from canopy flux measurements: An assessment of uncertainties and inter-algorithm variability. *Biogeosciences*, *14*(23), 5571–5594. https://doi.org/10.5194/bg-14-5571-2017

Langford, B., Cash, J. M., Vieno, M., Heal, M. R., Drewer, J., Jones, M. R., et al. (2022). Evaluation of isoprene light response curves for bryophyte-dominated ecosystems and implications for atmospheric composition. *Environmental Research: Ecology*, *2*(1), 011002. https://doi.org/10.1088/2752-664x/aca2ad

Langford, B., Misztal, P. K., Nemitz, E., Davison, B., Helfter, C., Pugh, T. A., et al. (2010). Fluxes and concentrations of volatile organic compounds from a south-East Asian tropical rainforest. *Atmospheric Chemistry and Physics*, *10*(17), 8391–8412. https://doi.org/10.5194/acp-10-8391-2010

Li, T., Baggesen, N., Seco, R., & Rinnan, R. (2023). Seasonal and diel patterns of biogenic volatile organic compound fluxes in a subarctic tundra. *Atmospheric Environment*, *292*, 119430. https://doi.org/10.1016/j.atmosenv.2022.119430

Li, Y., Liu, B., Ye, J., Jia, T., Khuzestani, R. B., Sun, J. Y., et al. (2021). Unmanned aerial vehicle measurements of volatile organic compounds over a subtropical forest in China and implications for emission heterogeneity. *ACS Earth and Space Chemistry*, *5*(2), 247–256. https://doi.org/10.1021/acsearthspacechem.0c00271

Marais, E. A., Jacob, D. J., Guenther, A. B., Chance, K., Kurosu, T. P., Murphy, J. G., et al. (2014). Improved model of isoprene emissions in Africa using Ozone Monitoring Instrument (OMI) satellite observations of formaldehyde: Implications for oxidants and particulate matter. *Atmospheric Chemistry and Physics*, *14*(15), 7693–7703. https://doi.org/10.5194/acp-14-7693-2014

Misztal, P. K., Nemitz, E., Langford, B., Di Marco, C. F., Phillips, G. J., Hewitt, C. N., et al. (2011). Direct ecosystem fluxes of volatile organic compounds from oil palms in south-East Asia. *Atmospheric Chemistry and Physics*, *11*(17), 8995–9017. https://doi.org/10.5194/acp-11-8995-2011

Monson, R. K., Harley, P. C., Litvak, M. E., Wildermuth, M., Guenther, A. B., Zimmerman, P. R., & Fall, R. (1994). Environmental and developmental controls over the seasonal pattern of isoprene emission from Aspen leaves. *Oecologia*, *99*(3–4), 260–270. https://doi.org/10.1007/bf00627738

Monson, R. K., Weraduwage, S. M., Rosenkranz, M., Schnitzler, J.-P., & Sharkey, T. D. (2021). Leaf isoprene emission as a trait that mediates the growth-defense tradeoff in the face of climate stress. *Oecologia*, *197*(4), 885–902. https://doi.org/10.1007/s00442-020-04813-7

Mota de Oliveira, S., Duijm, E., Stech, M., Ruijgrok, J., Polling, M., Barbosa, C. G., et al. (2022). Life is in the air: An expedition into the Amazonian atmosphere. *Frontiers in Ecology and Evolution*, *10*, 789791. https://doi.org/10.3389/fevo.2022.789791

Nagori, J., Janssen, R. H., Fry, J. L., Krol, M., Jimenez, J. L., Hu, W., & Vilà-Guerau de Arellano, J. (2019). Biogenic emissions and land–atmosphere interactions as drivers of the daytime evolution of secondary organic aerosol in the southeastern US. *Atmospheric Chemistry and Physics*, *19*(2), 701–729. https://doi.org/10.5194/acp-19-701-2019

Nepstad, D. C., de Carvalho, C. R., Davidson, E. A., Jipp, P. H., Lefebvre, P. A., Negreiros, G. H., et al. (1994). The role of deep roots in the hydrological and carbon cycles of Amazonian forests and pastures. *Nature*, *372*(6507), 666–669. https://doi.org/10.1038/372666a0

Niinemets, Ü., Arneth, A., Kuhn, U., Monson, R. K., Peñuelas, J., & Staudt, M. (2011). The emission factor of volatile isoprenoids: Stress, acclimation, and developmental responses. *Biogeosciences*, *7*(7), 2203–2223. https://doi.org/10.5194/bg-7-2203-2010

Oku, H., Fukuta, M., Iwasaki, H., Tambunan, P., & Baba, S. (2008). Modification of the isoprene emission model G93 for Tropical Tree Ficus virgata. *Atmospheric Environment*, *42*(38), 8747–8754. https://doi.org/10.1016/j.atmosenv.2008.08.036

Opacka, B., Müller, J.-F., Stavrakou, T., Bauwens, M., Sindelarova, K., Markova, J., & Guenther, A. B. (2021). Global and regional impacts of land cover changes on isoprene emissions derived from spaceborne data and the MEGAN Model. *Atmospheric Chemistry and Physics*, *21*(11), 8413–8436. https://doi.org/10.5194/acp-21-8413-2021

Opacka, B., Müller, J.-F., Stavrakou, T., Miralles, D. G., Koppa, A., Pagán, B. R., et al. (2022). Impact of drought on isoprene fluxes assessed using field data, satellite-based gleam soil moisture and HCHO observations from OMI. *Remote Sensing*, *14*(9), 2021. https://doi.org/10.3390/rs14092021

Otu-Larbi, F., Bolas, C. G., Ferracci, V., Staniaszek, Z., Jones, R. L., Malhi, Y., et al. (2020). Modelling the effect of the 2018 summer heatwave and drought on isoprene emissions in a UK woodland. *Global Change Biology*, *26*(4), 2320–2335. https://doi.org/10.1111/gcb.14963

Palmer, P. I., Marvin, M. R., Siddans, R., Kerridge, B. J., & Moore, D. P. (2022). Nocturnal survival of isoprene linked to formation of upper tropospheric organic aerosol. *Science*, *375*(6580), 562–566. https://doi.org/10.1126/science.abg4506

Perkins-Kirkpatrick, S. E., Alexander, L. V., & Nairn, J. R. (2012). Increasing frequency, intensity and duration of observed global heatwaves and warm spells. *Geophysical Research Letters*, *39*(20), L20714. https://doi.org/10.1029/2012gl053361

Perkins-Kirkpatrick, S. E., & Lewis, S. C. (2020). Increasing trends in regional heatwaves. *Nature Communications*, *11*(1), 3357. https://doi.org/10.1038/s41467-020-16970-7

Pétron, G., Harley, P., Greenberg, J., & Guenther, A. (2001). Seasonal temperature variations influence isoprene emission. *Geophysical Research Letters*, *28*(9), 1707–1710. https://doi.org/10.1029/2000gl011583

Pfister, G. G., Emmons, L. K., Hess, P. G., Lamarque, J.-F., Orlando, J. J., Walters, S., et al. (2008). Contribution of isoprene to chemical budgets: A model tracer study with the NCAR CTM mozart-4. *Journal of Geophysical Research*, *113*(D5), D05308. https://doi.org/10.1029/2007jd008948

Pike, R. C., & Young, P. J. (2009). How plants can influence tropospheric chemistry: The role of isoprene emissions from the Biosphere. *Weather*, *64*(12), 332–336. https://doi.org/10.1002/wea.416

Potosnak, M. J., LeStourgeon, L., Pallardy, S. G., Hosman, K. P., Gu, L., Karl, T., et al. (2014). Observed and modeled ecosystem isoprene fluxes from an oak-dominated temperate forest and the influence of drought stress. *Atmospheric Environment*, *84*, 314–322. https://doi.org/10.1016/j.atmosenv.2013.11.055

Saleska, S. R., Miller, S. D., Matross, D. M., Goulden, M. L., Wofsy, S. C., da Rocha, H. R., et al. (2003). Carbon in Amazon forests: Unexpected seasonal fluxes and disturbance-induced losses. *Science*, *302*(5650), 1554–1557. https://doi.org/10.1126/science.1091165

Sarkar, C., Guenther, A. B., Park, J.-H., Seco, R., Alves, E., Batalha, S., et al. (2020). PTR-TOF-MS eddy covariance measurements of isoprene and monoterpene fluxes from an eastern Amazonian rainforest. *Atmospheric Chemistry and Physics*, *20*(12), 7179–7191. https://doi.org/10.5194/acp-20-7179-2020

Sarkar, C., Guenther, A. B., Park, J.-H., Seco, R., Alves, E., Batalha, S., et al. (2022). 2014 Tapajos Brazil PTRTOFMS isoprene fluxes [Dataset]. *UCI BAI - Data Archive*. https://bai.ess.uci.edu/research/data-archive

Seco, R., Holst, T., Davie-Martin, C. L., Simin, T., Guenther, A., Pirk, N., et al. (2022). Strong isoprene emission response to temperature in tundra vegetation. *Proceedings of the National Academy of Sciences of the USA*, *119*(38), e2118014119. https://doi.org/10.1073/pnas.2118014119

Seco, R., Holst, T., Matzen, M. S., Westergaard-Nielsen, A., Li, T., Simin, T., et al. (2020). Volatile organic compound fluxes in a subarctic peatland and lake. *Atmospheric Chemistry and Physics*, *20*(21), 13399–13416. https://doi.org/10.5194/acp-20-13399-2020

Seco, R., Karl, T., Guenther, A., Hosman, K. P., Pallardy, S. G., Gu, L., et al. (2015). Ecosystem-scale volatile organic compound fluxes during an extreme drought in a broadleaf temperate forest of the Missouri Ozarks (central USA). *Global Change Biology*, *21*(10), 3657–3674. https://doi.org/10.1111/gcb.12980

Sharkey, T. D., Wiberley, A. E., & Donohue, A. R. (2008). Isoprene emission from plants: Why and how. *Annals of Botany*, *101*(1), 5–18. https://doi.org/10.1093/aob/mcm240

Sharkey, T. D., Yeh, S., Wiberley, A. E., Falbel, T. G., Gong, D., & Fernandez, D. E. (2005). Evolution of the isoprene biosynthetic pathway in kudzu. *Plant Physiology*, *137*(2), 700–712. https://doi.org/10.1104/pp.104.054445

Silva, S. J., Heald, C. L., & Guenther, A. B. (2020). Development of a reduced-complexity plant canopy physics surrogate model for use in chemical transport models: A case study with GEOS-chem V12.3.0. *Geoscientific Model Development*, *13*(6), 2569–2585. https://doi.org/10.5194/gmd-13-2569-2020

Situ, S., Wang, X., Guenther, A. B., Zhang, Y., Wang, X., Huang, M., et al. (2014). Uncertainties of isoprene emissions in the Megan model estimated for a coniferous and broad-leaved mixed forest in southern China. *Atmospheric Environment*, *98*, 105–110. https://doi.org/10.1016/j.atmosenv.2014.08.023

Sprengnether, M., Demerjian, K. L., Donahue, N. M., & Anderson, J. G. (2002). Product analysis of the OH oxidation of isoprene and 1,3-butadiene in the presence of NO. *Journal of Geophysical Research*, *107*(D15). https://doi.org/10.1029/2001jd000716

Stanton, N. A., & Tandon, N. F. (2023). How does tropospheric VOC chemistry affect climate? An investigation of preindustrial control simulations using the community Earth system model version 2. *Atmospheric Chemistry and Physics*, *23*(16), 9191–9216. https://doi.org/10.5194/acp-23-9191-2023

Su, L., Patton, E. G., Vilà-Guerau de Arellano, J., Guenther, A. B., Kaser, L., Yuan, B., et al. (2016). Understanding isoprene photooxidation using observations and modeling over a subtropical forest in the southeastern US. *Atmospheric Chemistry and Physics*, *16*(12), 7725–7741. https://doi.org/10.5194/acp-16-7725-2016

Tang, J., Chen, S., Martín Belda, D., Rinnan, R., Körner, C., & Fu, Y. H. (2024). Air and surface temperatures differently drive terrestrial carbon and water cycles in the high latitudes. *Geophysical Research Letters*, *51*(19), e2024GL110652. https://doi.org/10.1029/2024gl110652

Tang, J., Schurgers, G., Valolahti, H., Faubert, P., Tiiva, P., Michelsen, A., & Rinnan, R. (2016). Challenges in modelling isoprene and monoterpene emission dynamics of arctic plants: A case study from a subarctic tundra heath. *Biogeosciences*, *13*(24), 6651–6667. https://doi.org/10.5194/bg-13-6651-2016

The International GEOS-Chem User Community. (2021). GEOS-Chem classic (GCClassic) 13.3.3 (Version 13.3.3) [Software]. https://doi.org/10.5281/zenodo.5748260

Tiiva, P., Faubert, P., Michelsen, A., Holopainen, T., Holopainen, J. K., & Rinnan, R. (2008). Climatic warming increases isoprene emission from a subarctic heath. *New Phytologist*, *180*(4), 853–863. https://doi.org/10.1111/j.1469-8137.2008.02587.x

Trainer, M., Williams, E. J., Parrish, D. D., Buhr, M. P., Allwine, E. J., Westberg, H. H., et al. (1987). Models and observations of the impact of natural hydrocarbons on rural ozone. *Nature*, *329*(6141), 705–707. https://doi.org/10.1038/329705a0

Vettikkat, L., Miettinen, P., Buchholz, A., Rantala, P., Yu, H., Schallhart, S., et al. (2023). High emission rates and strong temperature response make boreal wetlands a large source of isoprene and terpenes. *Atmospheric Chemistry and Physics*, *23*(4), 2683–2698. https://doi.org/10.5194/acp-23-2683-2023

Wang, H., Lu, X., Seco, R., Stavrakou, T., Karl, T., Jiang, X., et al. (2022). Modeling isoprene emission response to drought and heatwaves within MEGAN using evapotranspiration data and by coupling with the Community Land Model. *Journal of Advances in Modeling Earth Systems*, *14*(12), e2022MS003174. https://doi.org/10.1029/2022ms003174

Wang, H., Nagalingam, S., Welch, A. M., Leong, C., Czimczik, C. I., & Guenther, A. B. (2024). Heat waves may trigger unexpected surge in aerosol and ozone precursor emissions from sedges in urban landscapes. *Proceedings of the National Academy of Sciences*, *121*(45), e2412817121. https://doi.org/10.1073/pnas.2412817121

Wang, H., Welch, A., Nagalingam, S., Leong, C., Kittitananuvong, P., Barsanti, K. C., et al. (2024a). Arctic heatwaves could significantly influence the isoprene emissions from shrubs. *Geophysical Research Letters*, *51*(2), e2023GL107599. https://doi.org/10.1029/2023gl107599

Wang, H., Welch, A. M., Nagalingam, S., Leong, C., Czimczik, C. I., Tang, J., et al. (2024b). High temperature sensitivity of Arctic isoprene emissions explained by sedges. *Nature Communications*, *15*(1), 6144. https://doi.org/10.1038/s41467-024-49960-0

Wei, D., Cao, C., Karambelas, A., Mak, J., Reinmann, A., & Commane, R. (2024). High-resolution modeling of summertime biogenic isoprene emissions in New York City. *Environmental Science & Technology*, *58*(31), 13783–13794. https://doi.org/10.1021/acs.est.4c00495

Wilkinson, M. J., Owen, S. M., Possell, M., Hartwell, J., Gould, P., Hall, A., et al. (2006). Circadian control of isoprene emissions from oil palm (*elaeis guineensis*). *The Plant Journal*, *47*(6), 960–968. https://doi.org/10.1111/j.1365-313x.2006.02847.x

Wu, J., Albert, L. P., Lopes, A. P., Restrepo-Coupe, N., Hayek, M., Wiedemann, K. T., et al. (2016). Leaf development and demography explain photosynthetic seasonality in Amazon evergreen forests. *Science*, *351*(6276), 972–976. https://doi.org/10.1126/science.aad5068

Xiong, F., McAvey, K. M., Pratt, K. A., Groff, C. J., Hostetler, M. A., Lipton, M. A., et al. (2015). Observation of isoprene hydroxynitrates in the southeastern United States and implications for the fate of NOx. *Atmospheric Chemistry and Physics*, *15*(19), 11257–11272. https://doi.org/10.5194/acp-15-11257-2015

Xu, T., White, L., Hui, D., & Luo, Y. (2006). Probabilistic inversion of a terrestrial ecosystem model: Analysis of uncertainty in parameter estimation and model prediction. *Global Biogeochemical Cycles*, *20*(2), GB2007. https://doi.org/10.1029/2005gb002468

Yáñez-Serrano, A. M., Nölscher, A. C., Williams, J., Wolff, S., Alves, E., Martins, G. A., et al. (2015). Diel and seasonal changes of biogenic volatile organic compounds within and above an Amazonian rainforest. *Atmospheric Chemistry and Physics*, *15*(6), 3359–3378. https://doi.org/10.5194/acp-15-3359-2015

Yang, Y., Bloom, A. A., Ma, S., Levine, P., Norton, A., Parazoo, N. C., et al. (2021). CARDAMOM-FluxVal Version 1.0 [Software]. https://doi.org/10.5281/zenodo.4904195

Yang, Y., Bloom, A. A., Ma, S., Levine, P., Norton, A., Parazoo, N. C., et al. (2022). CARDAMOM- FluxVal version 1.0: A FLUXNET-based validation system for CARDAMOM carbon and water flux estimates. *Geoscientific Model Development*, *15*(4), 1789–1802. https://doi.org/10.5194/gmd-15-1789-2022

Ziehn, T., Scholze, M., & Knorr, W. (2012). On the capability of Monte Carlo and adjoint inversion techniques to derive posterior parameter uncertainties in terrestrial ecosystem models. *Global Biogeochemical Cycles*, *26*(3), GB3025. https://doi.org/10.1029/2011gb004185

References From the Supporting Information

Andreae, M. O., Acevedo, O. C., Araùjo, A., Artaxo, P., Barbosa, C. G., Barbosa, H. M., et al. (2015). The Amazon tall tower observatory (ATTO): Overview of pilot measurements on ecosystem ecology, meteorology, trace gases, and aerosols. *Atmospheric Chemistry and Physics*, *15*(18), 10723–10776. https://doi.org/10.5194/acp-15-10723-2015

Bolas, C. G., Ferracci, V., Robinson, A. D., Mead, M. I., Nadzir, M. S., Pyle, J. A., et al. (2020). IDIRAC: A field-portable instrument for long-term autonomous measurements of isoprene and selected vocs. *Atmospheric Measurement Techniques*, *13*(2), 821–838. https://doi.org/10.5194/amt-13-821-2020

Butt, N., Campbell, G., Malhi, Y., Morecroft, M., Fenn, K., & Thomas, M. (2009). *Initial results from establishment of a long-term broadleaf monitoring plot at Wytham Woods*. University of Oxford.

Carlton, A. G., de Gouw, J., Jimenez, J. L., Ambrose, J. L., Attwood, A. R., Brown, S., et al. (2018). Synthesis of the southeast atmosphere studies: Investigating fundamental atmospheric chemistry questions. *Bulletin of the American Meteorological Society*, *99*(3), 547–567. https://doi.org/10.1175/bams-d-16-0048.1

Chance, K., & Martin, R. V. (2017). The levenberg-marquardt method. In *Spectroscopy and radiative transfer of planetary atmospheres* (pp. 130–131). Oxford University Press.

Gelaro, R., McCarty, W., Suárez, M. J., Todling, R., Molod, A., Takacs, L., et al. (2017). The modern-era retrospective analysis for research and applications, version 2 (MERRA-2). *Journal of Climate*, *30*(14), 5419–5454. https://doi.org/10.1175/jcli-d-16-0758.1

Kljun, N., Calanca, P., Rotach, M. W., & Schmid, H. P. (2015). A simple two-dimensional parameterisation for Flux Footprint Prediction (FFP). *Geoscientific Model Development*, *8*(11), 3695–3713. https://doi.org/10.5194/gmd-8-3695-2015

Langford, B., Acton, W., Ammann, C., Valach, A., & Nemitz, E. (2015). Eddy-covariance data with low signal-to-noise ratio: Time-lag determination, uncertainties and limit of detection. *Atmospheric Measurement Techniques*, *8*(10), 4197–4213. https://doi.org/10.5194/amt-8-4197-2015

Levenberg, K. (1944). A method for the solution of certain non-linear problems in least squares. *Quarterly of Applied Mathematics*, *2*(2), 164–168. https://doi.org/10.1090/qam/10666

Madsen, K., Nielsen, H. B., & Tingleff, O. (2004). Methods for non-linear least squares problems. In *Lecture notes, informatics and mathematical modelling* (2nd ed.). Technical University of Denmark.

Marquardt, D. W. (1963). An algorithm for least-squares estimation of nonlinear parameters. *Journal of the Society for Industrial and Applied Mathematics*, *11*(2), 431–441. https://doi.org/10.1137/0111030

Wells, K. C., Millet, D. B., Payne, V. H., Deventer, M. J., Bates, K. H., de Gouw, J. A., et al. (2020). Satellite isoprene retrievals constrain emissions and atmospheric oxidation. *Nature*, *585*(7824), 225–233. https://doi.org/10.1038/s41586-020-2664-3